



# LUND UNIVERSITY

## Single Junction and Tandem Junction Nanowire Solar Cells

Alcer, David

2024

*Document Version:*  
Publisher's PDF, also known as Version of record

[Link to publication](#)

*Citation for published version (APA):*  
Alcer, D. (2024). *Single Junction and Tandem Junction Nanowire Solar Cells*. [Doctoral Thesis (compilation), Faculty of Engineering, LTH]. Department of Physics, Lund University.

*Total number of authors:*  
1

*Creative Commons License:*  
CC BY

### General rights

Unless other specific re-use rights are stated the following general rights apply:  
Copyright and moral rights for the publications made accessible in the public portal are retained by the authors and/or other copyright owners and it is a condition of accessing publications that users recognise and abide by the legal requirements associated with these rights.

- Users may download and print one copy of any publication from the public portal for the purpose of private study or research.
- You may not further distribute the material or use it for any profit-making activity or commercial gain
- You may freely distribute the URL identifying the publication in the public portal

Read more about Creative commons licenses: <https://creativecommons.org/licenses/>

### Take down policy

If you believe that this document breaches copyright please contact us providing details, and we will remove access to the work immediately and investigate your claim.

LUND UNIVERSITY

PO Box 117  
221 00 Lund  
+46 46-222 00 00

# Single Junction and Tandem Junction Nanowire Solar Cells

DÁVID ALCER

DEPARTMENT OF PHYSICS | FACULTY OF ENGINEERING | LUND UNIVERSITY





# Single Junction and Tandem Junction Nanowire Solar Cells

by Dávid Alcer



**LUND**  
UNIVERSITY

Thesis for the degree of Doctor of Philosophy

To be presented, with the permission of the Faculty of Engineering at Lund University,  
for public criticism in the Rydberg lecture hall (Rydbergsalen) at the Department of Physics  
on Friday, the 19<sup>th</sup> of April 2024 at 09:15.

*Thesis advisor*

Professor Magnus T. Borgström

*Supporting advisors*

Professor Mats-Erik Pistol, Associate Professor Jesper Wallentin

*Faculty opponent*

Professor Jos E. M. Haverkort

Eindhoven University of Technology, Netherlands

|  |  |  |       |
|--|--|--|-------|
| Organization<br><b>LUND UNIVERSITY</b><br>Department of Physics<br>Box 118<br>SE-221 00 LUND<br>Sweden   |  | Document name<br><b>DOCTORAL DISSERTATION</b>                |       |
|  |  | Date of disputation<br>2024-04-19                            |       |
| Author(s)<br>Dávid Alcer   |  | Sponsoring organization                                      |       |
| Title and subtitle<br>Single Junction and Tandem Junction Nanowire Solar Cells   |  |  |       |
| Abstract<br><p>Solar cells based on silicon are successfully harvesting solar energy in established and increasingly widespread solar panels. However, their efficiency is limited by the Shockley–Queisser limit. For certain applications where high efficiency is the key figure of merit, the use of multi-junction solar cells is desirable.</p> <p>III–V multi-junction solar cells exhibit the highest efficiencies achieved to date, but suffer from the high cost of the III–V materials.</p> <p>Arrays of III–V nanowires show strong light absorption while covering only a small fraction of the surface, minimizing materials consumption. Therefore, solar cells made from III–V nanowire arrays are a possible candidate to achieve high efficiencies at a fraction of the cost of traditional planar III–V solar cells. This thesis aims to contribute to the development of III–V nanowire solar cells by addressing some of the challenges the technology is facing.</p> <p>Concerning single junction nanowire solar cells, Paper I investigates the effects of the device size on the performance. In contrast to the commonly used devices in nanowire solar cell research with an area below <math>1 \times 1 \text{ mm}^2</math>, significantly larger devices with an area of <math>10 \times 10 \text{ mm}^2</math> were processed, and the effects of device size on the external quantum efficiency (EQE) and <math>J</math>–<math>V</math> characteristics are investigated.</p> <p>A concept of optically transparent nanowire solar cells which can absorb near-infrared radiation is presented in Paper II.</p> <p>In the realm of nanowire synthesis, Paper III is a comparative study of two different Ga precursors to establish favorable conditions for the growth of GaInP nanowire segments. Paper IV reports on the successful processing of tandem junction nanowire solar cells based on a GaInP top junction and an InP bottom junction, connected by an Esaki tunnel diode.</p> |  |  |       |
| Key words<br>Nanowire solar cell, GaInP, InP, Tandem junction, Vertical processing   |  |  |       |
| Classification system and/or index terms (if any)  |  |  |       |
| Supplementary bibliographical information  |  | Language<br>English  |       |
| ISSN and key title   |  | ISBN<br>978-91-8039-960-9 (print)<br>978-91-8039-961-6 (pdf) |       |
| Recipient's notes  |  | Number of pages<br>95  | Price |
|  |  | Security classification                                      |       |

I, the undersigned, being the copyright owner of the abstract of the above-mentioned dissertation, hereby grant to all reference sources the permission to publish and disseminate the abstract of the above-mentioned dissertation.

Signature

Date 2024-03-21

# Single Junction and Tandem Junction Nanowire Solar Cells

by Dávid Alcer



**LUND**  
UNIVERSITY

Division of Solid State Physics  
Department of Physics  
Faculty of Engineering  
Lund University

**Front cover illustration:** Artistic impression of the work presented in this thesis, based on the tale of giants and lakes in the popular science summary. Artwork by Johanna Alcer.

**Back cover illustration:** Scanning electron microscopy (SEM) image of Koji, recorded by the author. Koji is a culinary mold used for making Miso, soy sauce and Sake. To learn more about it, visit <https://fermentedaway.blogspot.com/> where further SEM images are shown as well.

Pages i–xx, 1–62 © 2024 Dávid Alcer

Paper I © 2023 The authors. Published by IOP Publishing. Licensed under CC-BY 4.0.

Paper II © 2021 AIP Publishing.

Paper III © 2023 The authors. Published by Wiley-VCH. Licensed under CC-BY 4.0.

Paper IV © 2024 The authors. Published by American Chemical Society. Licensed under CC-BY 4.0.

Division of Solid State Physics  
Department of Physics  
Faculty of Engineering  
Lund University

Box 118  
SE-221 00 LUND  
Sweden

ISBN: 978-91-8039-960-9 (print)

ISBN: 978-91-8039-961-6 (pdf)

Printed in Sweden by Media-Tryck, Lund University, Lund 2024



Media-Tryck is a Nordic Swan Ecolabel certified provider of printed material. Read more about our environmental work at [www.mediatryck.lu.se](http://www.mediatryck.lu.se)

**MADE IN SWEDEN** 

# Contents

|  |             |
|--|-------------|
| <b>Popular Science Summary:</b>  |             |
| <b>A Tale of Giants and Lakes</b>                                      | <b>iii</b>  |
| <b>Populärvetenskaplig sammanfattning:</b>                             |             |
| <b>En saga om jättar och sjöar</b>                                     | <b>ix</b>   |
| <b>Abstract</b>  | <b>xv</b>   |
| <b>Acknowledgments</b>   | <b>xvii</b> |
| <b>List of Publications</b>  | <b>xix</b>  |
| <b>1 Introduction</b>  | <b>1</b>    |
| 1.1 Outline . . . . .  | 3           |
| <b>2 Background</b>  | <b>5</b>    |
| 2.1 Working Principles of Semiconductors Solar Cells . . . . .         | 5           |
| 2.2 Si Solar Cells . . . . .   | 7           |
| 2.3 Thin Film and Emerging Solar Cell Technologies . . . . .           | 8           |
| 2.4 III–V Solar Cells . . . . .  | 10          |
| 2.5 III–V Nanowires . . . . .  | 11          |
| 2.6 III–V Nanowire Solar Cells . . . . .                               | 12          |
| <b>3 Nanowire Synthesis and Characterization</b>                       | <b>17</b>   |
| 3.1 Substrate Patterning . . . . .                                     | 17          |
| 3.2 Nanowire Growth by MOVPE . . . . .                                 | 18          |
| 3.3 Characterization of Nanowire Arrays . . . . .                      | 20          |
| <b>4 Processing and Characterization of Nanowire Solar Cells</b>       | <b>27</b>   |
| 4.1 Processing of Nanowire Solar Cells . . . . .                       | 27          |
| 4.2 Characterization of Nanowire Solar Cells . . . . .                 | 30          |
| 4.3 Large Area Nanowire Solar Cells – Results of Paper I . . . . .     | 33          |
| 4.4 Peel-Off of Nanowire Arrays . . . . .                              | 34          |
| 4.5 Peel-Off of Semi-Transparent Nanowire Arrays – Results of Paper II | 35          |

|  |           |
|--|-----------|
| <b>5 GaInP/InP Tandem Junction Nanowire Solar Cells</b>  | <b>37</b> |
| 5.1 Working Principles of Tandem Junction Solar Cells . . . . .  | 37        |
| 5.2 MOVPE Growth of GaInP – Results of Paper III . . . . .   | 40        |
| 5.3 Processing and Characterization of GaInP/InP Tandem Junction<br>Nanowire Solar Cells – Results of Paper IV . . . . . | 43        |
| <b>6 Outlook</b>   | <b>47</b> |
| <b>References</b>  | <b>49</b> |
| <b>Scientific publications</b>   | <b>63</b> |
| Paper I: Processing and characterization of large area InP nanowire<br>photovoltaic devices . . . . .                    | 65        |
| Paper II: Semiconductor nanowire array for transparent photovoltaic<br>applications . . . . .                            | 67        |
| Paper III: Comparison of triethylgallium and trimethylgallium precurs-<br>ors for GaInP nanowire growth . . . . .        | 69        |
| Paper IV: Vertically processed GaInP/InP tandem-junction nanowire<br>solar cells . . . . .                               | 71        |

# Popular Science Summary: A Tale of Giants and Lakes

Once upon a time, in a village not too far away, the town found itself in a peculiar situation. It was the early afternoon on a sunny and tranquil summer day, and a drowsy mood had spread among the inhabitants when the village was visited by giants. You should know that giants look just like you and me, only quite a bit larger. Not all of the giants are the same – some are taller, others shorter (but still *really* tall). Their arrival spread fear among the inhabitants of the village, who went into hiding, intimidated by the giants. At sunset the giants disappeared – to general relief – but only to return regularly from then on, visiting the village every day the sun was shining. Soon, people understood that their fears had been entirely groundless. Giants are some of the most friendly and helpful beings imaginable, and well-meaning towards the villagers. To help the village, the giants started to work relentlessly. But despite all attempts to persuade them to engage in a variety of tasks, there seemed to be just a single thing the giants wanted to do. It was a monotonous and exhausting task: lifting buckets of water from the local lake and emptying them high up on the hillside.

*As you may have guessed, this tale has an application to my topic of research and can be read as a direct translation of the mysterious world of solar cell physics into the no less mysterious world of giants. If you prefer to read on about the giants and don't want to be bothered by physics comments, feel free to skip the parts in italics.*

To come up with a use for the water lifted by the giants, the villagers decided to build a reservoir lake to catch the water and make use of its energy with a water wheel. The giants rejoiced at the idea that their monotonous labor of lifting water would soon become so valuable to the villagers. The prestigious master builder Ingmar Parker (short: InP) was invited to construct the reservoir and water wheel, with great success. Every (sunny) day, the giants lifted buckets of



**Figure 1:** Giants lifting buckets of water and pouring it into the hillside reservoir constructed by InP.

water to the reservoir, powering the water wheel and supplying the village with energy to mill their flour, as shown in Figure 1.

*Each giant represents light particles (called photons) of a certain energy, corresponding to a specific color of light. A photon can lift an electron by the amount of energy that the photon has. Just like a tall giant lifts that bucket of water higher up than a shorter giant. The structure constructed by InP corresponds to a semiconductor, which has a so-called valence band filled with electrons (the lake) and a mostly empty conduction band (the hillside reservoir). Indium phosphide (InP) is a semiconductor material from which solar cells can be made.*

Before long, however, the taller one of the giants, called Blue, could not get rid of a thought that had come to their mind. The water they lifted high up every time fell down a long way before splashing (almost violently) into the water reservoir constructed by InP. What a waste! On the other hand, the shorter giant called Red was just tall enough to gently discharge their bucket of water into the lake, which is much more efficient, isn't it?

*The goal in constructing an efficient solar cell is to make the most use of the energy provided by all the photons of all different colors. The Blue giant has discovered the issue of energy loss through thermalization. The electrons excited by high-energy (blue) photons lose their extra energy above the band gap energy. They only contribute the same amount of energy as all other absorbed photons,*

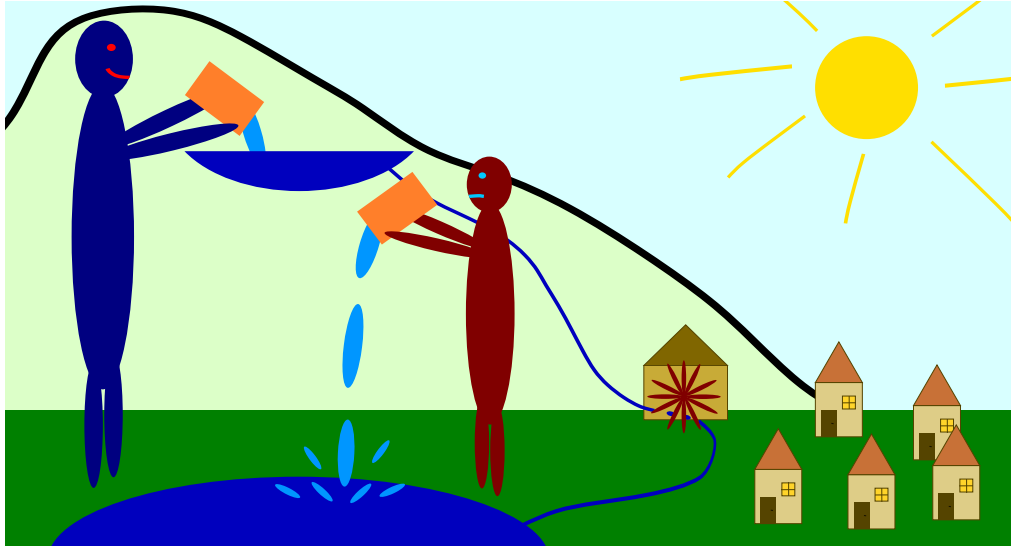


**Figure 2:** This reservoir constructed by GaInP is so high up that only the Blue giant reaches high enough to pour water into it.

*namely the band gap energy of the semiconductor material, in this case indium phosphide (InP).*

After discussing back and forth, the villagers invited the sister of Ingmar Parker, the equally famous master builder Gabi Ingrid Parker (short: GaInP). GaInP came up with the solution to move the reservoir higher up the hillside, which would make better use of the Blue giant's lifting work. The modification was quickly implemented, resulting in the structure shown in Figure 2. This made the Blue giant really happy – they could finally make advantage of their impressive height and seamlessly discharge each bucket of water into the reservoir high up the hill. Quite the contrary for the Red giant, however. Suddenly, they were not tall enough to reach all the way up to the reservoir, and their water-lifting effort was entirely useless! The villagers were not quite convinced either. The water from the reservoir high up put a lot of pressure on the water wheel, but there was much less water than previously, canceling out the benefits.

*The Red giant is unhappy for a good reason. Photons with too little energy are not able to lift an electron across the band gap of the semiconductor, and are thus not absorbed at all. This can be referred to as the loss of sub-band gap photons. Gallium indium phosphide (GaInP) is a semiconductor with a larger band gap than InP, which means less thermalization losses, but more losses of sub-band gap photons.*

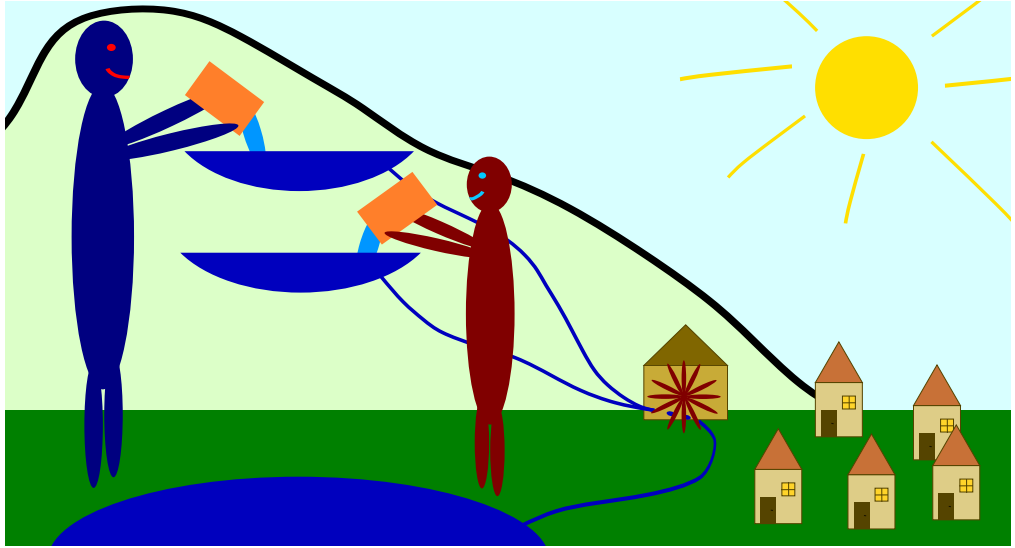


**Figure 3:** The Blue giant pours water into the higher reservoir, and the Red giant into the lower one. This tandem structure with two reservoirs is the most efficient!

The villagers (and not least the giants) argued about what to do, at what height to place the reservoir to best utilize the energy provided by the giants. Of course, in reality, unlike in the sketches shown here, the giants come in all colors of the rainbow, so that there will be some happy and some unhappy giants no matter what height you place the reservoir at. As it turned out, the original solution provided by InP was close to the optimum reservoir height, and the villagers settled for it, despite continuous grumbling from the Blue giant.

*A solar cell based on a single band gap semiconductor has to balance the two issues of thermalization losses and the loss of sub-band gap photons. The optimal efficiency attainable is called the Shockley–Queisser limit. InP happens to have a near-ideal band gap for a solar cell.*

Years later, after plenty of time to reconsider their life choices, the Blue giant came up with an idea. They urged the villagers to invite both siblings InP and GaInP to a new construction project, in order to build a tandem structure with two water reservoirs on the hillside. The Blue giant could pour water into the reservoir high up the hill constructed by GaInP, while the Red giant would use the InP reservoir further down the hill, as sketched in Figure 3. In this way, the lifting work of both giants would be used to the best extent possible. This ingenious idea was celebrated widely and caused lots of excitement among villagers and giants alike. The idea of the tandem structure was born!

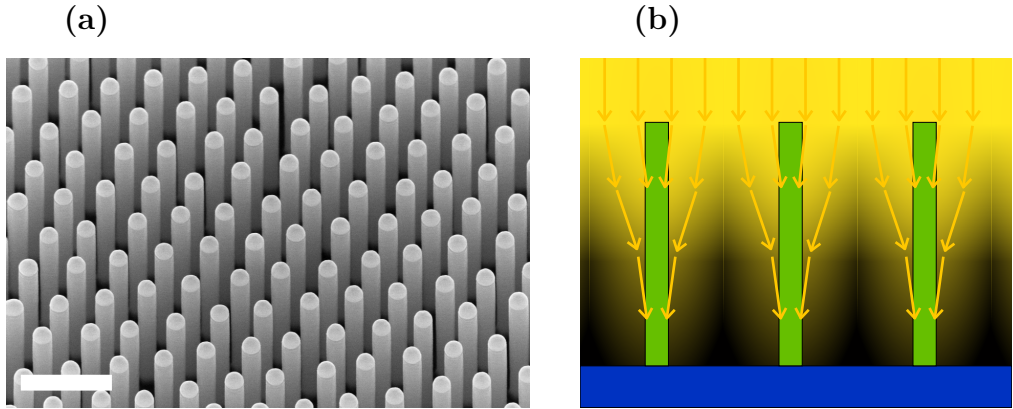


**Figure 4:** (a) Electron microscopy image of InP nanowires. Scale bar: 1000 nm. (b) Illustration of the light absorption in a nanowire array. The nanowires are shown in green, the substrate in blue, and the yellow gradient and arrows represent the incoming light that is sucked into the nanowires and absorbed.

*By combining semiconductor materials of different band gaps in a tandem junction solar cell, the energy of the photons of different colors can be used more efficiently, because thermalization losses as well as the losses of sub-band gap photons are reduced. In this way, the Shockley–Queisser limit can be exceeded. My thesis work is focused on constructing a tandem junction solar cell based on InP and GaInP.*

*Because InP and GaInP are very expensive materials, we want to use as little of them as possible. This is possible by using them in the form of nanowires, as seen in Figure 4 (a). Nanowires are very very thin rods (about 500 times thinner than your hair), and quite short as well, meaning that very little material is used. The nanowires nevertheless absorb the incoming light efficiently. As illustrated in Figure 4 (b), the strong absorption is possible because the incoming light behaves like a wave. It does not travel straight through the space between the nanowires, but is rather sucked into the nanowires. For this effect to work, the distance between the nanowires has to be very small, approximately as large as the wavelength of the light, which is the case for the nanowires seen in Figure 4 (a) as well as the nanowire arrays that I used for making solar cells. The results presented in this thesis are a step towards GaInP/InP tandem junction nanowire solar cells – I was able to make such solar cells work! However, due to several imperfections, they are not very efficient yet, and plenty of work remains to be done.*

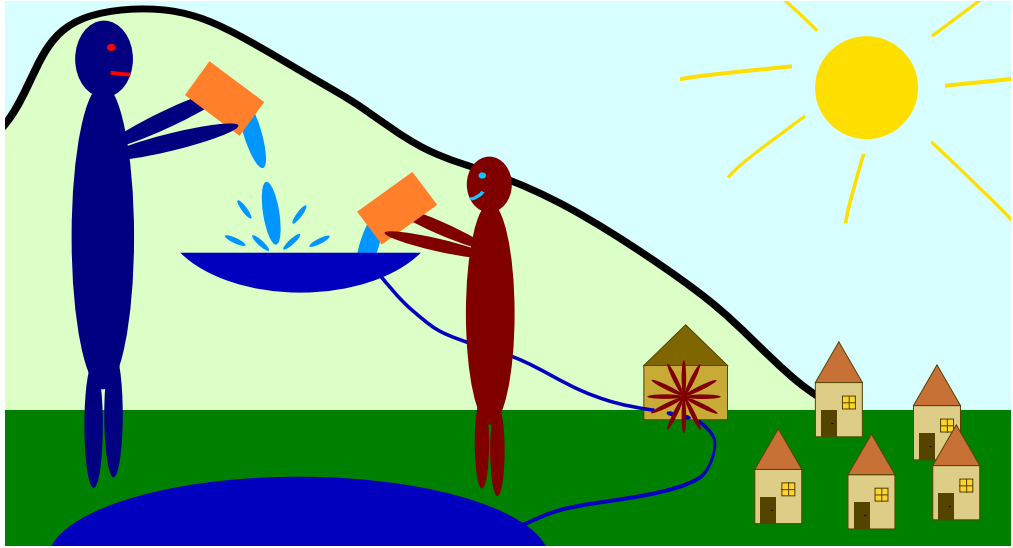


# Populärvetenskaplig sammanfattning: En saga om jättar och sjöar

Det var en gång, i en by inte alltför långt borta, som man en vacker dag fann sig i en märklig situation. Det var en solig och fridfull sommardag, och en dåsig stämning hade spridit sig bland invånarna, när byn fick besök av jättar. Du ska veta att jättar ser ut precis som du och jag, bara lite större. Alla är inte likadana – vissa jättar är längre, andra kortare (men ändå *väldigt* långa). Deras ankomst spred skräck bland byns invånare, som gömde sig eftersom de var rädda för jättarna. Vid solnedgången försvann jättarna – till allmän lättnad – men de återvände sedan regelbundet och besökte byn varje dag solen sken. Snart förstod byborna att deras rädsla hade varit helt grundlös. Jättar är några av de mest vänliga och hjälpsamma varelser man kan tänka sig, och de var välmenande mot byborna. För att hjälpa byn började jättarna arbeta outtröttligt. Men trots alla försök att övertala dem att ägna sig åt en mängd olika uppgifter verkade det bara finnas en enda sak som jättarna ville göra. Det var en monoton och utmattande uppgift, nämligen att lyfta hinkar med vatten från den lilla sjön och tömma dem högt uppe på bergssluttningen.

*Som du kanske har gissat vid det här laget har denna berättelse en tillämpning på mitt forskningsområde och kan läsas som en direkt översättning av solcells fysikens mystiska värld till jättarnas inte mindre mystiska värld. Om du föredrar att läsa om jättarna och inte vill bli störd av fysikkommentarer, så kan du helt enkelt hoppa över de kursiva delarna.*

För att komma på ett sätt att använda det vatten som jättarna lyfte beslutade byborna att bygga en reservoarsjö för att fånga upp vattnet och utnyttja dess energi med hjälp av ett vattenhjul. Jättarna jublade vid tanken på att deras monotona arbete med att lyfta vatten snart skulle bli så värdefullt för byborna. Den framstående byggmästaren Ingmar Persson (kort: InP) bjöds in för att bygga reservoaren och vattenhjulet, med stor framgång. Varje (solig) dag lyfte



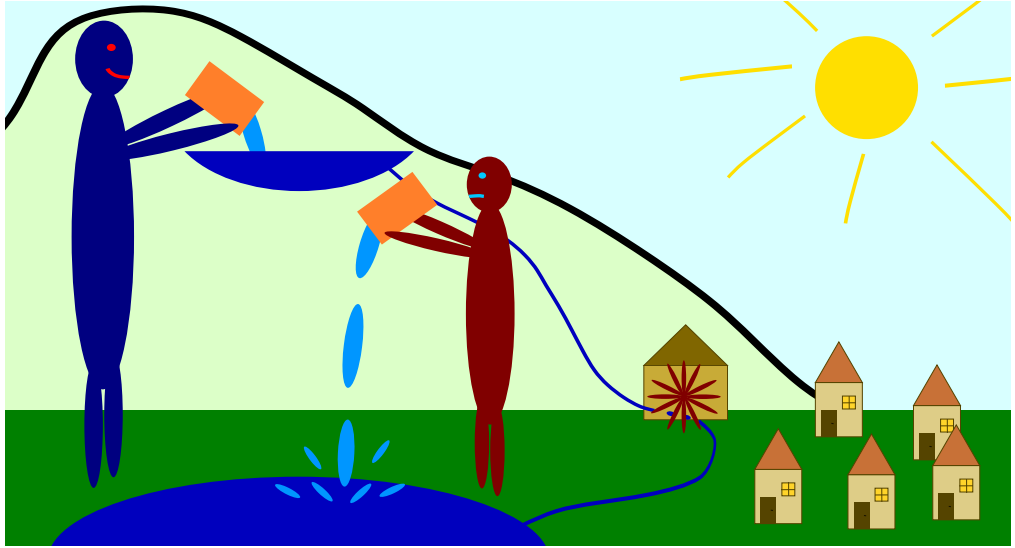
**Figur 1:** Jättar lyfter hinkar med vatten och häller det i den reservoar som InP har byggt på bergssluttningen.

jättarna hinkar med vatten till reservoaren, vilket drev vattenhjulet och försåg byn med energi för att mala sitt mjöl, vilket visas i figur 1.

*Varje jätte representerar ljuspartiklar (så kallade fotoner) med en viss energi, motsvarande en specifik ljusfärg. En foton kan använda sin mängd energi för att lyfta en elektron. Beroende på fotonens energi kan elektronen lyftas olika högt, precis som en lång jätte lyfter hinken med vatten högre upp än en kortare jätte. Den struktur som InP har byggt motsvarar en halvledare, som har ett så kallat valensband fyllt med elektroner (sjön) och ett i stort sett tomt ledningsband (reservoaren på berget). Indiumfosfid (InP) är ett halvledarmaterial av vilket man kan tillverka solceller.*

Det dröjde dock inte länge förrän den längre av jättarna, kallad Blå, inte kunde bli kvitt en tanke som hade slagit hen. Vattnet som hen lyfte upp föll ner en lång bit varje gång innan det slog ner (med ett ordentligt plask) i vattenreservoaren som InP hade byggt. Vad onödigt! Däremot var den kortare jätten Röd precis tillräckligt lång för att smidigt tömma sin hink med vatten i sjön, vilket är mycket mer effektivt, eller hur?

*Målet med att konstruera en effektiv solcell är att på bästa sätt utnyttja den energi som kommer från alla fotoner i alla olika färger. Jätten Blå har upptäckt problemet med energiförlust genom termalisering. Elektronerna som exciteras av högenergetiska (blå) fotoner förlorar sin extra energi utöver bandgapsenergin.*

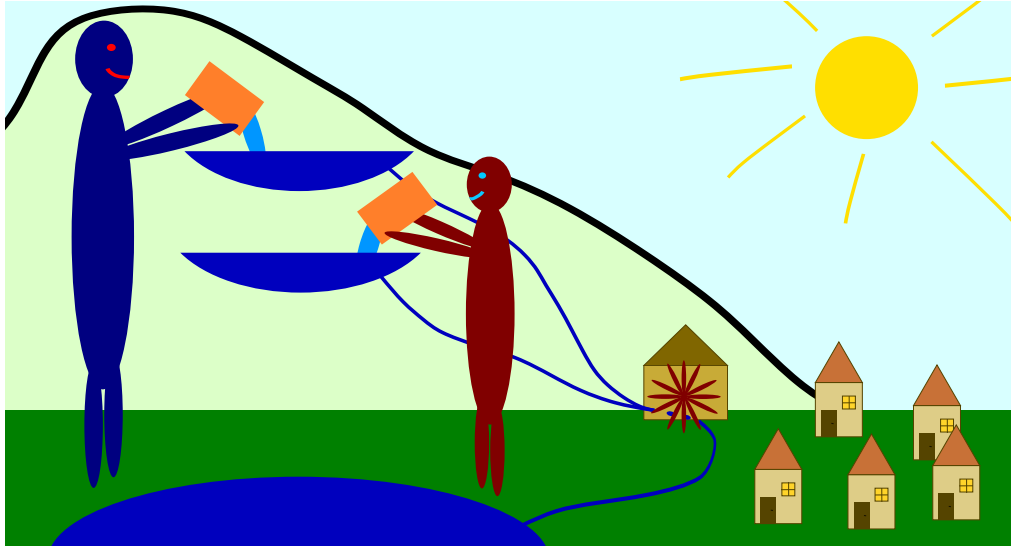


**Figur 2:** Denna reservoar som GaInP har byggt är så högt upp att endast jätten Blå når tillräckligt högt för att hålla vatten i den.

*De kommer endast att bidra med lika mycket energi som alla andra absorberade fotoner, nämligen bandgapsenergin i halvledarmaterialet, i det här fallet indiumfosfid (InP).*

Efter att ha diskuterat fram och tillbaka bjöd byborna in Ingmar Perssons system, den lika berömda byggmästaren Gabi Ingrid Persson (kort: GaInP). GaInP kom på lösningen att flytta reservoaren högre upp på sluttningen, vilket skulle göra det möjligt att bättre utnyttja lyftarbetet från jätten Blå. Denna modifiering genomfördes snabbt och resulterade i den struktur som visas i figur 2. Detta gjorde jätten Blå riktigt glad – hen kunde äntligen dra nytta av sin imponerande längd och sömlöst tömma varje hink med vatten i reservoaren högt upp på berget. Men för jätten Röd var det tvärtom. Plötsligt var hen inte tillräckligt lång för att nå hela vägen upp till reservoaren, och hens ansträngningar att lyfta vatten var helt värdelösa! Byborna var inte heller helt övertygade. Vattnet från reservoaren högt upp gav ett stort tryck på vattenhjulet, men det var mycket mindre vatten än tidigare, vilket upphävde fördelarna.

*Jätten Röd har god anledning till sitt missnöje. Fotoner med för låg energi kan inte lyfta en elektron över halvledarens bandgap och absorberas därför inte alls. Galliumindiumfosfid (GaInP) är en halvledare med ett större bandgap än InP, vilket innebär mindre energiförlust genom termalisering, men mer förluster av fotoner som har lägre energi än bandgapet.*

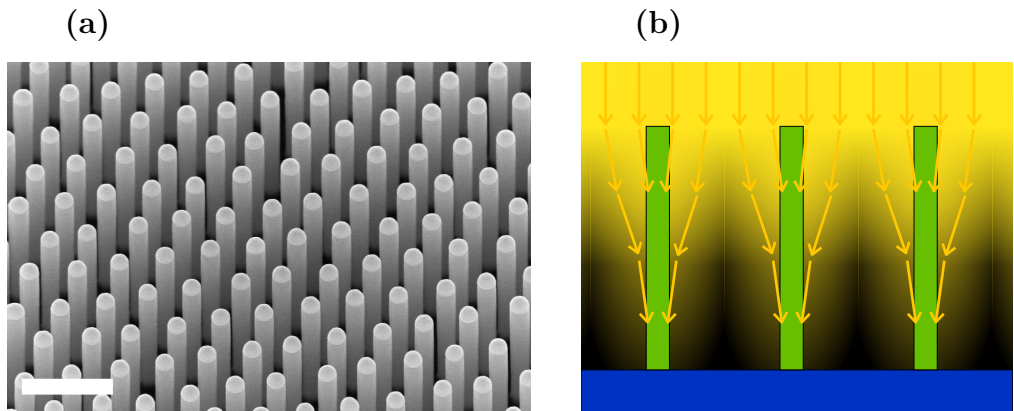


**Figur 3:** Jätten Blå håller vatten i den högre reservoaren, jätten Röd i den lägre. Denna tandemkonstruktion med två reservoarer är mest effektiv!

Byborna (och inte minst jättarna) diskuterade vad de skulle göra, på vilken höjd de skulle placera reservoaren för att på bästa sätt utnyttja den energi som jättarna tillhandahöll. I verkligheten, till skillnad från skisserna som visas här, finns jättarna naturligtvis i alla regnbågens färger, så det kommer att finnas några glada och några besvikna jättar oavsett vilken höjd man placerar reservoaren på. Det visade sig att den ursprungliga lösningen från InP låg nära den optimala höjden för reservoaren, och byborna nöjde sig med den, trots att det hördes fortsatt gnäll från jätten Blå.

*En solcell baserad på en enda halvledare måste balansera de två problemen med termaliseringsförluster och förlust av fotoner med en energi under bandgapet. Den optimala verkningsgrad som kan uppnås kallas Shockley–Queisser-gränsen, och beror på bandgapet. InP råkar ha ett nästan idealiskt bandgap för en solcell.*

Flera år senare, efter att ha funderat över sina livsval, kom jätten Blå på en idé. Hen uppmanade byborna att bjuda in båda syskonen InP och GaInP till ett nytt byggprojekt för att bygga en tandemstruktur med två vattenreservoarer på bergssluttningen. Jätten Blå kunde hålla vatten i den reservoar som GaInP konstruerat högt uppe på berget, medan jätten Röd kunde använda InP:s reservoar som låg lite längre ned, se figur 3. På så sätt utnyttjades båda jättarnas lyftarbete på bästa möjliga sätt. Denna genialiska idé firades rejält och väckte stor glädje bland byborna och jättarna. Idén om tandemstrukturen var född!



**Figur 4:** (a) InP-nanotrådar sedda i ett elektronmikroskop. Skalstreck: 1000 nm. (b) Illustration av ljusabsorptionen i en nanotrådsmatris. Nanotrådarna visas med grön färg, substratet i blått, och den gula ljusgradienten samt pilarna symboliserar det inkommande ljuset som sugts in i nanotrådarna och absorberas.

*Genom att kombinera halvledarmaterial med olika bandgap i en så kallad tandemsolcell, kan energin i fotoner med olika färg utnyttjas mer effektivt, eftersom förluster genom termalisering samt förluster av fotoner med lägre bandgap minskar. På så sätt kan Shockley–Queisser-gränsen överskridas. Mitt avhandlingsarbete är inriktat på att konstruera en tandemsolcell baserad på GaInP och InP.*

*Eftersom InP och GaInP är mycket dyra material vill vi använda så lite av dem som möjligt. Detta är möjligt genom att använda dem i form av nanotrådar, som visas i figur 4 (a). Nanotrådar är mycket mycket tunna stavar (ca 500 gånger tunnare än ett hårstrå), och dessutom ganska korta, vilket innebär att mycket lite material går åt. Men de absorberar ändå det inkommande ljuset på ett effektivt sätt. Som illustreras i figur 4 (b) är den starka absorptionen möjlig eftersom det inkommande ljuset beter sig som en våg. Det färdas inte rakt genom utrymmet mellan nanotrådarna, utan sugts snarare in i nanotrådarna. För att denna effekt ska fungera måste avståndet mellan nanotrådarna vara mycket litet, ungefär lika stort som ljusets våglängd, vilket är fallet för nanotrådarna i figur 4 (a) samt för nanotrådsmatriserna som jag använde för att tillverka solceller. Resultaten som presenteras i denna avhandling är ett steg mot GaInP/InP-tandemsolceller gjorda av nanotrådar – jag lyckades få sådana solceller att fungera! På grund av ett antal brister är de dock inte särskilt effektiva ännu, och mycket arbete återstår.*



# Abstract

Solar cells based on silicon are successfully harvesting solar energy in established and increasingly widespread solar panels. However, their efficiency is limited by the Shockley–Queisser limit. For certain applications where high efficiency is the key figure of merit, the use of multi-junction solar cells is desirable.

III–V multi-junction solar cells exhibit the highest efficiencies achieved to date, but suffer from the high cost of the III–V materials.

Arrays of III–V nanowires show strong light absorption while covering only a small fraction of the surface, minimizing materials consumption. Therefore, solar cells made from III–V nanowire arrays are a possible candidate to achieve high efficiencies at a fraction of the cost of traditional planar III–V solar cells. This thesis aims to contribute to the development of III–V nanowire solar cells by addressing some of the challenges the technology is facing.

Concerning single junction nanowire solar cells, Paper I investigates the effects of the device size on the performance. In contrast to the commonly used devices in nanowire solar cell research with an area below  $1 \times 1 \text{ mm}^2$ , significantly larger devices with an area of  $10 \times 10 \text{ mm}^2$  were processed, and the effects of device size on the external quantum efficiency (EQE) and  $J$ – $V$  characteristics are investigated.

A concept of optically transparent nanowire solar cells which can absorb near-infrared radiation is presented in Paper II.

In the realm of nanowire synthesis, Paper III is a comparative study of two different Ga precursors to establish favorable conditions for the growth of GaInP nanowire segments. Paper IV reports on the successful processing of tandem junction nanowire solar cells based on a GaInP top junction and an InP bottom junction, connected by an Esaki tunnel diode.



# Acknowledgments

The past 5 years working on my PhD project have been an exciting and most rewarding journey, made possible by the support of so many people around me.

First of all, I want to thank Magnus, my supervisor, for giving me the opportunity to work on this exciting and challenging project. Thank you for all discussions and guidance you provided, while also giving me the freedom to steer the direction of my research. Your supervision has allowed and encouraged me to grow in many different ways during my time as a PhD student.

I'm grateful to all former and current group members for collaborating, providing hands-on help, discussions and support. Thank you Yuwei and Lukas for taking the time to teach me the many different processes involved in fabricating nanowire arrays and making solar cells from them. It was a pleasure to work together with Kristi, Yue, Matteo, Mariia, Enrique, Aditya, Javier, Reza, Michael, Erik and Fatematuj. I'm also thankful for all the exchange of ideas during collaborations, with among others Thomas, Nelia, Austin, Vidar, Abhijit, Nils, Anders, Joachim, Xianshao, Arkady, Abbey and Bo.

When NanoLund and FTF claim to be a "Great place to do nanoscience", it's not an empty phrase. Thanks to all the wonderful people who can be enthusiastic or tired sometimes, sometimes chatty or sometimes lost in their own thoughts, but always manage to make me feel that FTF is a great place to belong. From research to teaching, collaborations to lunch chats in  $k$ -space, the open culture and friendly atmosphere around have given me new energy on many occasions. There are so many friends and colleagues I am thankful to!

Thank you to my fellow PhD students and postdocs Yue, Kristi, Matteo, Mariia, Enrique, Aditya, Javier, Jonatan, Oskar, Roman, Irene, David, Sven, Linnéa, Thanos, Julia, Anette, Asmita, Egor, Elke, Stephanie, Sebastian, Mokhtar, Esra, Elham, Max, Frida, Therese, Sara, Harald, Hossein, Marie, Enrico, Jason,

Markus, Marcus, Patrik, Pau, Ruby, Simon, Thea, Viktor, William and many more. Thank you Yue for being such a great office mate.

Thank you to all the faculty members, and especially Magnus, Mats-Erik, Jesper, Adam, Dan, Carina, Knut, Anders, Maria, Ville, Martin, and Hermann.

A big thanks also to the lab staff for keeping the cleanroom running and up to date! Thank you Bengt, Anders, Håkan, Luke, George, Natalia, Mariusz, Sarah, Peter, Alex, Emil, Sungyon, Maria, David and Dmitry.

I am thankful to the administrative and IT support as well as the cleaning staff, all helping to make FTF a nice workplace. Thank you Gerda, Mirja, Alexandra, Karin, Anneli, Anastasiia, Marica, Anna-Karin, Anna, Evelina, Line, Therese, Alfons, Andreas.

Finally, a huge thanks to all my friends (both at and outside of FTF) as well as my family, especially Fredrica, for your continuous support and encouragement! Of course, Johanna deserves an extra thanks for her artistic interpretation of my thesis for the front cover.

# List of Publications

This thesis is based on the following publications, referred to by their Roman numerals:

**I Processing and characterization of large area InP nanowire photovoltaic devices**

**D. Alcer**, L. Hrachowina, D. Hessman, and M. T. Borgström  
Nanotechnology 34, 295402 (2023)

I processed the nanowire solar cells and performed the presented measurements on the devices. I analyzed the data and was main responsible for the writing of the paper.

**II Semiconductor nanowire array for transparent photovoltaic applications**

Y. Chen, L. Hrachowina, E. Barrigon, J. P. Beech, **D. Alcer**, R. Lyttleton, R. Jafari Jam, L. Samuelson, H. Linke, and M. T. Borgström  
Applied Physics Letters 118, 191107 (2021)

I assisted Y. Chen in the fabrication of the nanowire arrays used in this study and contributed to the writing of the paper.

**III Comparison of triethylgallium and trimethylgallium precursors for GaInP nanowire growth**

**D. Alcer**, A. P. Saxena, L. Hrachowina, X. Zou, A. Yartsev, and M. T. Borgström  
Physica Status Solidi B, 2000400 (2020)

I synthesized the investigated GaInP/InP nanowire arrays and performed the measurements of growth rate and composition with support by L. Hrachowina. I was main responsible for the data analysis and the writing of the paper.

#### IV Vertically processed GaInP/InP tandem-junction nanowire solar cells

**D. Alcer**, M. Tirrito, L. Hrachowina, and M. T. Borgström  
ACS Applied Nano Materials 7, 2352–2358 (2024)

I synthesized the GaInP/InP tandem junction nanowire arrays with support by L. Hrachowina. I performed the XRD and PL measurements on the nanowire arrays, processed them into solar cells, and performed the EQE and  $J-V$  measurements on the devices. I analyzed the data and was main responsible for the writing of the paper.

All papers are reproduced with permission of their respective publishers.

Publications not included in this thesis:

#### **Growth of branched nanowires via solution-based Au seed particle deposition**

K. Adham, Y. Zhao, L. Hrachowina, **D. Alcer**, R. Wallenberg, and M. T. Borgström  
Materials Research Express 10, 085003 (2023)

I assisted K. Adham and Y. Zhao in the fabrication of the branched nanowire arrays used in this study and contributed to the writing of the paper.

# 1 Introduction

The excessive use of material and energy resources associated with Western lifestyles is rapidly destroying the planet’s ecosystems [1]. Persistently high levels of fossil fuel combustion threaten to irreversibly push the climate of the earth system into a hothouse state hostile to human life [2, 3]. Already now, climate disruption due to fossil fuel combustion is a key contributor to the high species extinction rates in what is termed the sixth mass extinction [4].

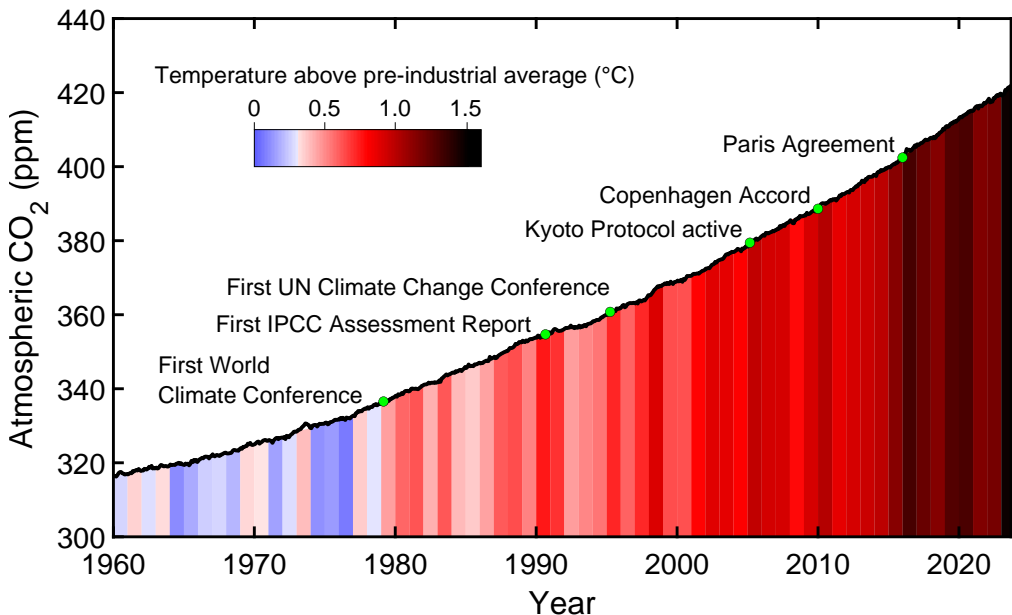


**Figure 1.1:** Atmospheric CO<sub>2</sub> concentration as a function of time between 1960 – 2023, measured at Mauna Loa [5]. The color coding of the bars is based on the yearly global average temperature obtained from Copernicus Climate Change Service [6]. Noteworthy climate conferences and agreements are indicated. In 2023, the global average temperature was 14.98 °C, which is 1.48 °C above the pre-industrial average [7].

Limiting global heating to 1.5 °C or 2 °C above the pre-industrial average could provide an (albeit uncertain) possibility to avoid triggering catastrophic climate tipping points [8]. However, the remaining carbon budget corresponding to these temperature increases is quickly diminishing. Under current emission levels, the carbon budget for a 66 % chance of staying below the 1.5 °C (or 2 °C) limit will be depleted within 2 (or 22) years [9]. Despite various climate agreements, no significant emission mitigation has been achieved [10], which is illustrated vividly by the so-called climate inaction stripes shown in Figure 1.1.

Central to the (quickly diminishing) prospect of navigating humanity into an ecologically safe and socially just space are rapid and profound lifestyle changes in high-consumption populations [11]. In addition, the transition from fossil fuels to renewable energies is a cornerstone of climate mitigation [12]. Solar energy harvested by use of photovoltaic modules, suitable for being deployed on a large scale, is the most promising source of renewable energy. In fact, solar photovoltaics amounts to three quarters of the renewable electricity capacity additions worldwide, the remainder being mostly wind energy [13]. Fueled by decreasing prices for silicon (Si) solar cells, the solar industry is growing significantly [14]. Figure 1.2 shows the global cumulative installed solar cell capacity, highlighting the near-exponential increase in solar cell installation.

Please note, however, that the increase in solar and other renewable energy generation has thus far only added to, and not substituted the use of fossil fuels at the global level [10]. To succeed in the energy transition, an accelerated deployment of renewable energy systems needs to be complemented with lifestyle changes, energy efficiency enhancements, and the early retirement of fossil fuel infrastructure [10].

Si is beyond doubt the cornerstone material for photovoltaics, mainly because large-scale manufacturing has led to decreasing prices, in combination with good efficiencies commonly approaching or exceeding 20 % for commercially available modules [16–18]. In combination with the fact that Si is very abundant in the Earth’s crust, this makes Si solar cells ideal for terrestrial electricity generation.

For niche applications where high efficiency is paramount, however, other concepts are needed. Solar cells made from III–V compound semiconductors surpass all other types of solar cells in terms of efficiency. When combining different III–V materials in a tandem junction solar cell, the Shockley–Queisser limit can be exceeded, which has made possible high efficiencies close to 40 % [19]. However, the high cost of the III–V substrates is prohibitive for most terrestrial applications.

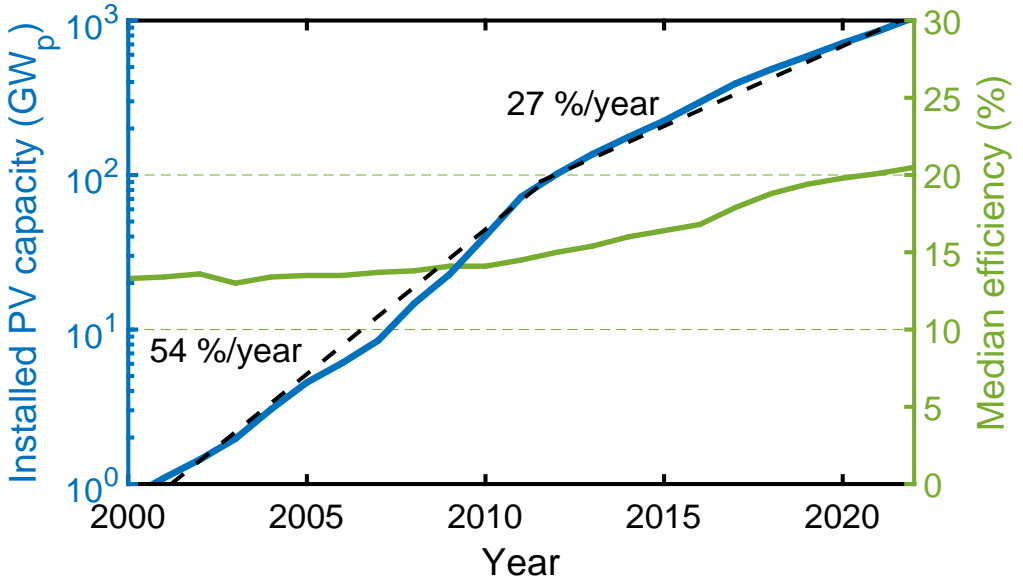


**Figure 1.2:** Semi-logarithmic plot of the global cumulative installed solar cell capacity (measured in terms of the peak power capacity) as a function of time (left axis, data from [15]). Medium solar conversion efficiency of Si solar panels in the US residential market (right axis, data from [16]).

One possible route towards high-efficiency solar cells at a lower cost than for planar III–V cells is the use of III–V nanowire arrays. Despite only covering a small fraction of the substrate area, arrays of III–V nanowires efficiently absorb the incoming sunlight [20, 21]. Promising results of high-efficiency III–V nanowire array solar cells have been achieved, reaching efficiencies around of 17 % [22–24]. However, to further push efficiencies and exceed the Shockley–Queisser limit, the adoption of a tandem junction architecture is needed [25].

## 1.1 Outline

In this thesis, work on the development of single junction and tandem junction nanowire solar cells is presented. The thesis consists of two main parts,

1. the so-called ‘kappa’ including chapters 1 – 6, and
2. the included scientific publications, Paper I – Paper IV.

Chapter 2 of the kappa provides a background to the presented work, where currently existing as well as emerging solar cell technologies are discussed. The state of research on III–V nanowires and their applications is also touched upon.

Chapters 3 and 4 describe the fabrication of InP nanowire array solar cells and a range of characterization techniques. In Chapter 3, the focus is on the synthesis of the nanowires and their characterization in the as-grown arrays. Chapter 4 describes the processing steps for fabricating nanowire solar cells, as well as the measurements performed on the processed devices. In this context, Paper I focuses on the processing and characterization of InP nanowire solar cells. Devices as large as  $10 \times 10 \text{ mm}^2$  have been processed, and the influence of device size on the performance was investigated. Paper II presents results on a novel concept of transparent solar cells, based on peeling off sparse photovoltaic nanowire arrays by embedding them in a polymer film. This enables good light absorption in the near-infrared spectral region, while being transparent in the visible.

Chapter 5 describes the progress on GaInP/InP tandem junction nanowire solar cells, with a focus on the working principles of tandem junction solar cells as well as their characterization. To support the growth of such nanowires, Paper III compares results from using two different Ga precursors for the GaInP nanowire segment synthesis. Paper IV focuses on the processing and characterization of tandem junction nanowire solar cell devices based on GaInP/InP nanowires, and presents the results achieved so far.

Finally, in Chapter 6, a brief outlook on the future development of nanowire solar cells is provided.

## 2 Background

The photovoltaic effect was first discovered by Edmond Becquerel in 1839 in an inadvertently realized copper-cuprous oxide thin-film solar cell [26]. However, unaware of the existence and properties of semiconductors, a theory of the effect was lacking well into the 20th century. The invention of semiconductor solar cells based on p–n junctions can be traced to Chapin et al. at Bell Labs, who realized a p–n junction single-crystalline Si solar cell [27].

### 2.1 Working Principles of Semiconductors Solar Cells

A semiconductor is a material characterized by its band gap  $E_g$ , the energy difference between the conduction band edge and the valence band edge [28]. In an intrinsic semiconductor at room temperature, the number of electrons in the conduction band and the number of holes (i.e. missing electrons in the valence band) are low, because thermal excitation of electrons across the band gap has a low statistical probability. The electron distribution  $F$  as a function of energy  $E$  is determined by the Fermi-Dirac distribution

$$F(E) = \frac{1}{e^{(E-E_F)/k_B T} + 1}$$

where  $k_B T$  is the thermal energy. The position of the Fermi level  $E_F$  relative to the conduction and valence band edges governs the distribution of electrons. In order to increase the conductivity of a semiconductor, the material can be doped, which shifts the Fermi level  $E_F$  close to the conduction or valence band edge. When doping with donors, an excess of electrons in the conduction band is created, corresponding to a position of the Fermi level  $E_F$  close to the conduction band edge. Similarly, doping with acceptors creates holes in the valence band. In both cases, the charge of the ionized dopant atoms is compensated for by the free electrons/holes.

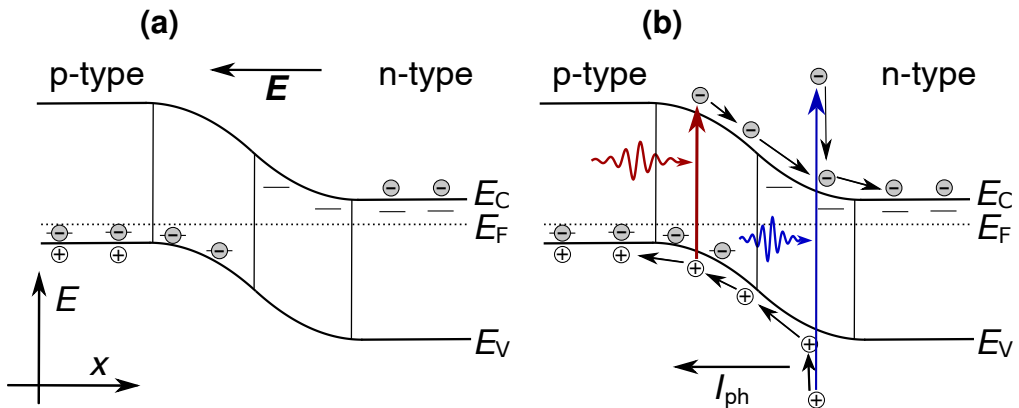


**Figure 2.1:** (a) Band diagram of a p–n junction under short-circuit conditions, showing a spatial dimension on the  $x$ -axis and energy on the  $y$ -axis. The ionized donors and acceptors in the depletion region around the p–n junction give rise to the built-in electric field  $\mathbf{E}$ . (b) Light absorption is possible for photon energies above the band gap of the semiconductor. For every absorbed photon, an electron is lifted from the conduction band to the valence band. The generated electrons and holes have an excess energy dependent on the absorbed photon energy, which is dissipated by charge carrier thermalization. The electrons (holes) generated within the depletion region drift towards the n-doped (p-doped) side due to the built-in electric field  $\mathbf{E}$ . Electrons and holes are extracted from the n-doped and p-doped sides respectively, generating the photocurrent  $I_{\text{ph}}$ .

A p–n junction is made up of an n-doped and a p-doped segment of a semiconductor matched together, as shown in Figure 2.1 (a). The Fermi level  $E_F$  is constant across the structure in thermal equilibrium, and is close to the conduction band edge in the n-type region and valence band edge in the p-type region, respectively. In the so-called depletion region located close to the junction, no free charge carriers are present due to the larger distance of the Fermi level  $E_F$  from the conduction/valence band edges. The charge of the ionized donors/acceptors thus leads to an electric field in the depletion region, called the built-in electric field, which in turn explains the bending of the conduction and valence band as seen in Figure 2.1.

When light impinges on the semiconductor, electrons in the valence band can absorb photons and be lifted to the conduction band, creating an electron–hole pair, as indicated in Figure 2.1 (b). This process is only possible if the photon energy  $\hbar\omega$  (where  $\omega$  is the angular frequency of the photon and  $\hbar$  the reduced Planck’s constant) exceeds the band gap of the semiconductor, such that photons with an energy  $\hbar\omega < E_g$  are not absorbed. The excess energy of absorbed photons  $\hbar\omega - E_g$  is transferred to kinetic energy of the electron

and hole and lost to thermalization of the hot carriers. Together with the loss of sub-band gap photons, the thermalization loss constitutes one of the most important factors limiting the efficiency of p–n junction solar cells. Further fundamental losses include Carnot loss<sup>1</sup> and entropy-related losses, such as entropy loss due to the spontaneous emission in a larger solid angle compared to the solid angle of the incident solar radiation [29]. Taking into account all these losses, the Shockley–Queisser limit describes the maximum achievable efficiency using a planar p–n junction solar cell as a function of the band gap of the used semiconductor [29, 30]. The maximum attainable Shockley–Queisser limit under one sun (AM 1.5G) illumination is 33 % at a band gap of  $E_g = 1.34$  eV [31].

The working principle of the p–n junction solar cell relies on the separation of the photogenerated electron-hole pairs in the built-in electric field of the p–n junction. The electrons and holes drift towards the n- and p-side of the junction, respectively, generating a reverse current, called photocurrent ( $I_{\text{ph}}$ ) or short-circuit current ( $I_{\text{SC}}$ ). To generate power, the p–n junction solar cell is operated under forward bias, while still generating the photocurrent  $I_{\text{ph}}$  in the reverse direction of the diode [32].

## 2.2 Si Solar Cells

Although the basic operating principle remained the same, Si solar cells have evolved significantly since their invention. In the early years, solar cells were used for powering spacecraft, leading to the development of a small but established solar cell industry focusing on reliable and efficient single-crystalline Si (c-Si) solar cells for spacecraft, with considerations of cost regarded as secondary. In the 1970s, the potential of solar cells for terrestrial applications became apparent, prompting the industry to prioritize cost reduction [26]. Consequently, solar cells made from cheaper polycrystalline Si wafers, as well as thin film solar cells became contestants to c-Si solar technology [33]. Recently, a dramatic reduction of Si photovoltaics (PV) cost, with a learning rate of about 20 % for each doubling in cumulative installed capacity [34], has driven an exponential growth of PV module deployment. Outperforming poly-Si as well as thin film technologies in terms of efficiency, c-Si dominates the terrestrial PV market to date and is expected to continue being the core technology in an exponentially expanding PV market in the near future [33].

---

<sup>1</sup>The Carnot loss is the thermodynamic loss resulting from the finite temperature of the Sun and of the Earth (and thus the solar panels). It is  $1 - \eta_{\text{max}} = \frac{T_{\text{Earth}}}{T_{\text{Sun}}} = \frac{300 \text{ K}}{5777 \text{ K}} = 5.2 \%$  where  $\eta_{\text{max}}$  is the Carnot efficiency of a heat engine operating between reservoirs with a temperature of  $T_{\text{Earth}}$  and  $T_{\text{Sun}}$ , respectively.

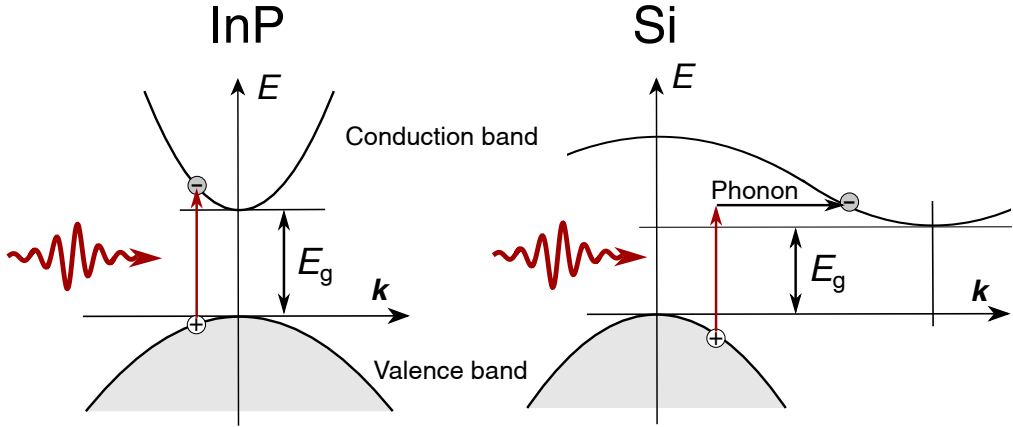


**Figure 2.2:** Schematically drawn band structure of a direct and an indirect band gap semiconductor, such as InP and Si, respectively. The absorption of light by excitation of an electron from the valence band to the conduction band is shown. For an indirect band gap semiconductor such as Si, the photon absorption requires simultaneous interaction with a phonon to bridge the mismatch in crystal momentum  $\mathbf{k}$ .

Recent developments have led to increased efficiency of solar modules by implementing innovations that have been demonstrated at lab-scale but were previously considered too costly for large-scale production. Most importantly, the introduction of the passivated emitter and rear contact (PERC) technology has led to increased module efficiencies of 21 – 22 % and largely replaced the previously dominant aluminum back surface field (BSF) technology [35]. Similarly, the introduction of new advancements including tunnel oxide passivated contacts (TOPCon) and interdigitated back contacts (IBCs) on n-type Si wafers are on the horizon [36]. With these innovations, Si solar modules are expected to eventually reach up to 25 – 26 % efficiency [35], matching the efficiencies of lab-scale record devices today [37, 38]. This efficiency is very close to the Shockley–Queisser limit of 29 % for a Si solar cell, limiting possibilities for further improvement [39].

### 2.3 Thin Film and Emerging Solar Cell Technologies

An intrinsic disadvantage of crystalline Si as a solar cell material is its indirect band gap, leading to weak absorption of light [40]. The difference between a direct and an indirect band gap semiconductor is the crystal momentum  $\mathbf{k}$  at which the energy maximum of the valence band and the energy minimum of the conduction band occur. For an indirect band gap semiconductor such as

Si, they are located at different values of  $\mathbf{k}$ . This is illustrated by Figure 2.2, where the process of light absorption is shown for a direct and an indirect band gap semiconductor. Because a photon carries energy, but no significant crystal momentum  $\mathbf{k}$ , the transfer of crystal momentum from a phonon is necessary for light absorption in an indirect band gap semiconductor such as Si, reducing the absorption probability. For complete light absorption and correspondingly highest possible efficiency, the industry standard for solar cell production is based on 160  $\mu\text{m}$  thick high-quality Si wafers [41]. Solar cells made from direct band gap semiconductors can be made much thinner, on the order of 1  $\mu\text{m}$  in thickness. The prospect of lower costs due to reduced materials usage has fueled research on a number of thin film solar cell technologies.

The most widespread commercially implemented thin film solar cell technologies are based on cadmium telluride (CdTe) and Cu(In,Ga)Se<sub>2</sub> (CIGS) [42]. However, problems with the reliability of the manufacturing process have caused increased costs as well as module efficiencies significantly below lab-scale device efficiency [43]. Additionally, concerns about the toxicity of cadmium for CdTe and the limited availability of indium for CIGS solar cells have hampered the wide-scale adoption of the technologies [42, 44]. After peaking at 17 % in 2009, the market share of thin film PV has stabilized at 5 % of the total global PV production today [33].

Dye-sensitized as well as organic solar cells are types of emerging PV and are based on selective charge carrier transfer. In dye-sensitized solar cells, electrons are transferred between the light-absorbing dye and titanium dioxide nanoparticles submerged in an electrolyte [42]. Organic solar cells, which are based on electron/hole selective contacts sandwiching the light-absorbing layer, have been pursued for the promise of large-area production at low cost, due to the possibility of depositing the organic layers using simple solution processing methods [42]. However, due to low efficiency (especially for large-area devices) and stability issues, organic solar cells are not yet commercially implemented [45].

Interest in emerging solar cells has recently concentrated predominantly on perovskite solar cells, due to the remarkably rapid increase of attainable efficiency from below 10 % in 2010 to exceeding 25 % in 2020 [46]. This success has been possible due to advantageous optoelectronic properties and defect tolerance of the inorganic halide perovskite materials used as absorbers [42, 47]. The instability and degradation of perovskite solar cells under exposure to oxygen, humidity, and UV radiation are well-known challenges, with a significant amount of efforts dedicated to address these issues, and promising results achieved recently [48–50]. Commercialization of high-efficiency perovskite-on-silicon tandem junction as well as single-junction perovskite solar cells is ongoing, driven by the compan-

ies Oxford PV (UK) and GCL Nano (CN), respectively [47]. However, concerns regarding the toxicity of the perovskite materials due to their content of lead (Pb) as well as long-term stability issues continue to threaten the prospects for perovskite solar cells [47, 48].

## 2.4 III–V Solar Cells

III–V semiconductors are a class of materials ideally suited for optoelectronic applications due to their direct band gap and high carrier mobility [51]. As a result, the highest photoconversion efficiencies between all types of solar cells are achieved using III–V semiconductors [52]. However, the shortcoming of III–V semiconductor materials is their high cost, especially driven by the cost of the generally used GaAs or Ge substrates [53]. This has limited the areas of application to the cost-insensitive fields of space PV and concentrator PV, where high efficiency is paramount [54, 55].

In order to surpass the Shockley–Queisser efficiency limit for single band gap solar cells, multi-junction cells comprising several p–n junctions made from III–V semiconductors with different band gap energies have been developed. Absorption of high-energy photons in the top junction semiconductor with the highest band gap reduces thermalization losses, and lower energy photons can be absorbed in the bottom junction semiconductor. While dual-junction (often lattice-matched GaInP/GaAs) and triple junction (often lattice-matched GaInP/GaAs/Ge) cells are the most common [56, 57], III–V solar cells with as many as 6 junctions have been developed, with a current efficiency record of 39.2 % under 1 Sun illumination (AM1.5G) [19].

Due to their high cost, III–V solar cells are not competitive in non-concentrator terrestrial applications. In particular, the thickness of the used III–V semiconductor wafers (on the order of 350  $\mu\text{m}$ ) means that a relatively large amount of expensive III–V material is needed, even when only the top few  $\mu\text{m}$  comprise the active PV device [58]. Attempts to tackle this problem include the growth of metamorphic III–V solar cells on Si substrates [59], and substrate removal and reuse strategies such as epitaxial lift-off [60]. Drawbacks of these strategies include thermal expansion coefficient mismatch between Si and III–V materials for metamorphic III–V on Si, limiting the device efficiency [59]. Concerning substrate removal and reuse, the need to prepare the substrate for subsequent growth cycles using chemical–mechanical polishing (CMP) limits the potential for cost reduction, ultimately preventing application in mainstream PV markets [60].

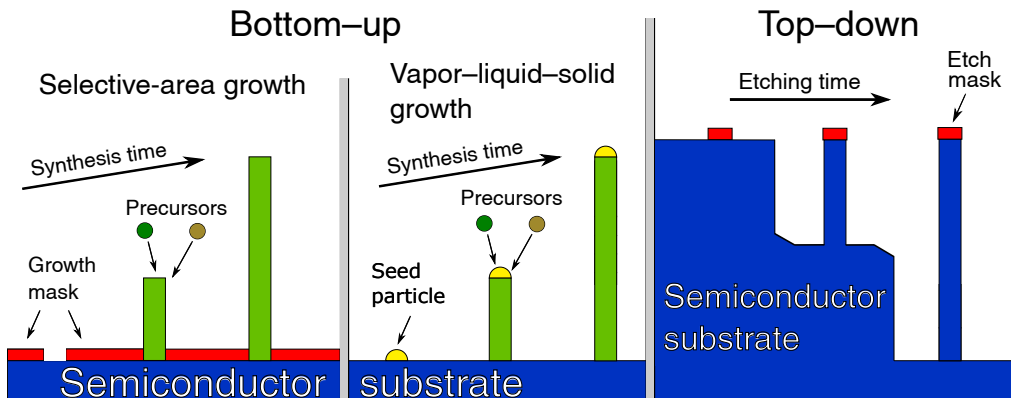


**Figure 2.3:** Modes of manufacturing nanowires: bottom-up and top-down approaches. Two bottom-up growth techniques are illustrated: selective area epitaxy and vapor-liquid-solid (VLS) growth.

## 2.5 III-V Nanowires

Semiconductor nanowires have attracted significant attention in the past two decades, due to a number of unique properties derived from the nanowire geometry [61]. Strain relaxation along the radial direction of the nanowire allows for the combination of lattice-mismatched materials to form axial heterostructures within a nanowire [62, 63].

Similarly, the small cross-section of the nanowires enables the growth of III-V nanowires directly on Si substrates [64]. Due to the superior optoelectronic properties of III-V semiconductors, in particular the high electron mobility compared to Si and their direct band gap, the integration of III-V semiconductors on Si is actively researched [65–68]. III-V nanowires present a possible path of realizing high-mobility III-V channels to overcome the limitations of Si field effect transistors [69–71]. The demand for optical chip-to-chip communication has further spurred research on nanowire photodetectors and lasers integrated on Si [72–74].

Nanowires can be manufactured using two distinctively different approaches, the top-down and the bottom-up approach, illustrated in Figure 2.3. In the top-down approach, high-quality bulk material is selectively etched to create the desired structure [75]. In the bottom-up approach, nanowires are synthesized from the constituent elements under appropriate conditions for crystal growth [75]. The inherent advantage of bottom-up synthesis is the added freedom of design, enabling various structures and materials combinations that are not attainable in bulk form, such as the previously mentioned axial heterostructures

of lattice-mismatched materials within a nanowire [62, 63]. Other examples include the synthesis of III–V nanowires with a metastable wurtzite (WZ) crystal structure which does not exist in bulk, and even axial crystal phase heterostructures with WZ and zinc-blende (ZB) segments [76, 77]. Methods for bottom-up nanowire synthesis include vapor–liquid–solid (VLS) growth, selective area epitaxy and aerotaxy [75], of which mainly Au-seeded VLS growth will be discussed in this thesis.

The VLS mechanism of crystal growth using Au seed particles was invented by Wagner and Ellis at Bell Labs, who used it to grow Si wires [78]. The field of III–V nanowires emerged in the 1990s after the VLS growth method was successfully applied to III–V semiconductors [79–81]. VLS nanowire growth is based on nanoparticles that facilitate the synthesis of a semiconductor crystal at the interface between the particle and the substrate. The term derives from the three phases involved in the synthesis – the vapor phase from which precursors are supplied, the (presumed) liquid phase of the seed particle, and the solid phase of the semiconductor crystal. Precursor atoms from the gas phase come in contact with the seed particle and alloy with it, leading to a supersaturation of the constituents atoms in the seed particle. This supersaturation drives the nanowire crystal growth at the particle–semiconductor interface. All the nanowire arrays that the work of this thesis is based on are synthesized using the VLS growth method with regularly placed Au seed particles.

In order to achieve the desired functionality, heterostructures of materials composition and doping within a nanowire are necessary. They can take the form of axial as well as radial heterostructures. Axial heterostructures are usually achieved by changing the provided precursor materials during the axially proceeding nanowire growth. Radial heterostructures, also called core–shell structures, are formed as a consecutive epitaxial step after the growth of the core nanowire, by tuning growth parameters to favor radial shell growth [75].

## 2.6 III–V Nanowire Solar Cells

Regular arrays of III–V nanowires have attracted attention as a promising approach to achieve highly efficient next-generation solar cells [75]. Due to their high refractive index and a diameter comparable to the wavelength of light, nanowires contain strongly confined waveguided modes. The optical antenna effect enables an efficient coupling of the incoming light to these confined optical modes, complemented by strong absorption due to the direct band gap of the used III–V semiconductors [82–84]. By designing an array of nanowires with

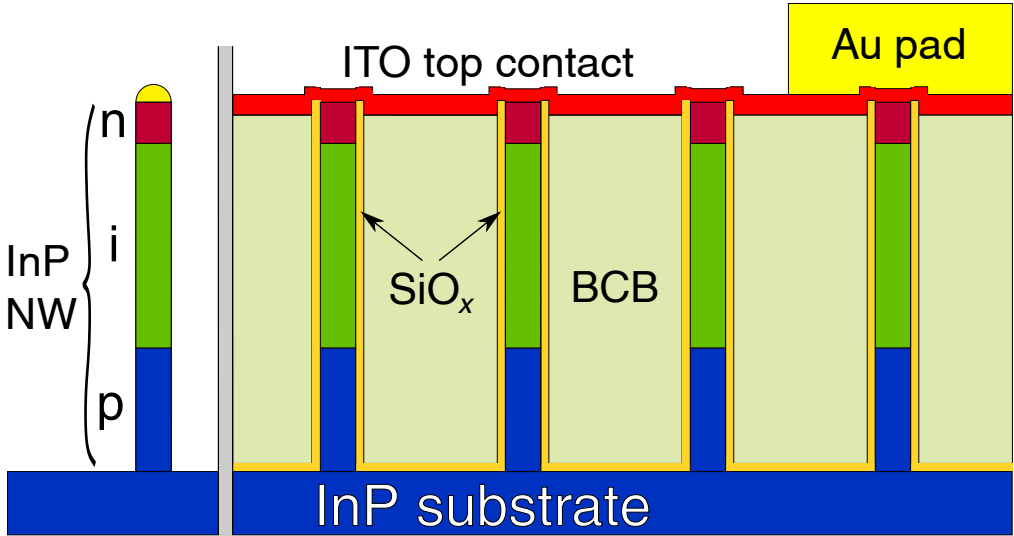


**Figure 2.4:** Schematic illustration of a single junction InP nanowire solar cell. On the left, a free-standing nanowire is shown. The structure of a vertically-processed nanowire solar cell is shown on the right. It contains a  $\text{SiO}_x$  passivating layer, BCB for planarization, and an indium tin oxide (ITO) transparent top contact. The device can be contacted via the Au pad on top, and a backside contact to the InP wafer.

proper pitch and diameter, almost complete absorption of the incoming visible light can be achieved with a nanowire length of just  $2\ \mu\text{m}$  [20, 21]. The structure of a nanowire solar cell is shown schematically in Figure 2.4, using the example of axial single junction InP nanowire solar cells as processed within the work presented in Chapter 4 as well as Paper I.

Interestingly, it has been shown that the single junction efficiency limit can be slightly higher for nanowire solar cells than the Shockley–Queisser limit for planar cells. As the emission from a nanowire array is directional, entropy losses due to emission into a large solid angle are reduced, increasing the theoretically attainable efficiency [85, 86].

The option of combining lattice-mismatched materials within a nanowire enables a wider freedom of design to tailor the band gap as compared to planar heterostructures. This is relevant in particular for axially defined tandem junction solar cells, where novel combinations of materials are possible in the nanowire geometry.

III–V nanowire solar cells have been shown experimentally as well as in simulations to withstand high-energy radiation better than planar cells made from

the same materials [87, 88]. Due to their nanoscale dimensions, collisions with high-energy particles are both less likely and induce fewer defects, as the collision cascades are truncated radially [88]. As radiation damage is an important concern for solar cells deployed in space, this makes III–V nanowire solar cells a promising candidate for space applications [88].

Due to the reduced materials requirement, III–V nanowire solar cells hold the promise of delivering an efficiency on par with their planar counterparts at substantially lower costs. Because III–V substrates are expensive, this requires a strategy that does not rely on the use of a new III–V substrate for each nanowire array growth cycle [89, 90].

One such strategy is to reuse the costly III–V substrate several times after peeling off the nanowire array in a polymer film [91–97]. Apart from the promise of cost reduction, such ultra-low weight thin film III–V nanowire solar cells embedded in the thin polymer film would provide added value in several ways. For space application, the low weight and resulting high specific power is an important figure of merit [87]. The flexible nature of the resulting polymer film embedded nanowire arrays also makes them interesting for building integrated photovoltaics. Furthermore, by manipulating the spacing and diameter of the nanowires, semi-transparent thin film solar cells can be envisioned, further increasing the potential field of applications within building integrated photovoltaics [98].

A different option is the direct growth of III–V nanowire array solar cells on Si. In this direction, the commonly pursued aim is to realize a III–V nanowire on Si tandem junction solar cell – promising an efficiency increase compared to Si solar cells, at potentially competitive added costs [25].

A third and distinctly different strategy is represented by Aerotaxy, a substrate-free growth method in which seed nanoparticles pass through the reactor while being suspended as an aerosol in the carrier gas [99]. By mixing the carrier gas with precursor gases in the heated reactor, nanowire growth at very high growth rates can be achieved, enabling mass production of III–V nanowires for solar cells [25, 100–102]. While superior in terms of growth rate and throughput, difficulties in accurately controlling the growth of complex heterojunction structures in Aerotaxy persist [102].

Concerning the design of photovoltaic nanowires, two distinct categories can be defined based on the direction of charge carrier separation. Axial junction solar cells contain a p–n junction in the axial direction of the nanowire, separating charge carriers between the bottom and top of the nanowires. On the other hand, radial junction nanowire solar cells are based on a core–shell structure in

which the charge carrier separation takes place between the differently doped nanowire core and shell [103]. This brings the advantage of a shorter distance for charge carrier separation, made possible by the decoupling of the axis of light absorption (axial) and the direction of charge carrier separation (radial) [24, 103]. This advantage weighs in mainly when the charge carrier lifetime in the nanowire material is short [24, 103].

To date, a wide range of different nanowire solar cells have been manufactured with respect to the choice of nanowire material, substrate, growth method and junction geometry [75]. Record efficiencies of around 17 % have been achieved by solar cells manufactured from arrays of InP nanowires [22–24], but also GaAs nanowire solar cells have been shown to reach an efficiency of up to 15.3 % [104]. Bottom-up synthesis using selective area growth as well as VLS growth using a Au seed particle have been used successfully [22, 104–106], as well as top-down manufacturing using selective etching of bulk InP [23, 24]. Axial nanowire solar cells generally achieve higher efficiencies than those based on a radial p-n junction and have thus been researched more extensively [75]. A noteworthy exception is a p-InP-core n-ZnO/AZO-multishell solar cell published by Raj et al. with an efficiency of 17.1 % [24]. While efforts have been made to manufacture III-V nanowire solar cells on graphene, Si, and using peeled-off nanowire arrays, the highest efficiencies are so far achieved using nanowires standing on their native substrate [75, 107–109].

With several different types of III-V nanowire solar cells exceeding an efficiency of 15 %, the technology has proven to be a promising contender in the hunt for highly efficient and affordable next-generation photovoltaics. However, a further increase of solar conversion efficiency is needed for the technology to become a competitive option compared to currently existing Si and planar III-V solar cells. To achieve efficiencies beyond the Shockley-Queisser limit, a tandem structure solar cell design is to be used [89]. A number of combinations for the top and bottom cell material exist with band gap energies that are suitable for tandem solar cells. Given the feature of radial strain relaxation, material combinations with relatively large lattice mismatch can be used. Most research towards tandem junction nanowire solar cells has been performed on the III-V nanowire on Si design, where only the top subcell is located in the nanowire, and the bottom subcell is planar Si [25, 109]. Several subcells located within the same nanowire have recently been grown successfully in our group, using the GaInP/InP and GaInP/InP/InAsP materials systems [110, 111].



# 3 Nanowire Synthesis and Characterization

## 3.1 Substrate Patterning

When aiming to create regular arrays of nanowires like those needed for nanowire solar cells, a lithography method capable of creating the corresponding nanoscale pattern is needed. The most commonly used patterning method in nanotechnology research, electron beam lithography, is not suitable for the creation of patterns stretching large areas due to its sequential nature. Therefore, we have used two lithography methods, nanoimprint lithography and displacement Talbot lithography, that are able to produce periodic patterns on wafer-scale areas in a parallel manner. Both methods are used successfully to define the hexagonal arrays of Au nanoparticles with a pitch of 500 nm and diameter of 180 – 200 nm which are used for most of the work in this thesis.

Nanoimprint lithography is a patterning technique that relies on physically structuring the resist during the lithography step. To achieve that, the stamp used for the lithography has three-dimensional features [112, 113]. When pressed against the substrate at a high pressure and elevated temperature, the resist layer on the substrate is molded, as the stamp creates holes in the resist [114]. A double-layer resist structure (LOR 0.7A/TU7-120) enables the widening of the hole in the bottom layer by use of a wet chemical etching step, see the scanning electron microscope (SEM) image in Figure 3.1 (a) for the resulting structure. The undercut creates a discontinuity in the evaporated Au film, such that all the Au on top of the resists can be removed by dissolving the resist layers in Microposit Remover 1165, and only the Au that is placed inside the holes will stay on the substrate – see Figure 3.1 (b) for the resulting array of Au particles. During the growth process, a nanowire will grow from each of these Au particles, leading to an array of vertical free-standing nanowires.

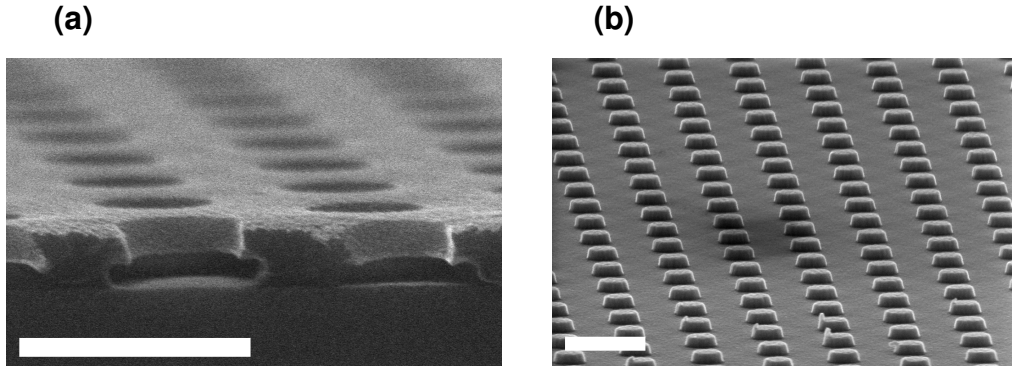


**Figure 3.1:** (a) Cross-sectional SEM image of the double layer resist structure prior to evaporating Au. During the nanoimprint lithography step, holes are created in the upper resist, TU7-120. An etching step using oxygen plasma widens the holes and removes remaining residues of TU7-120 from them. The bottom resist, LOR0.7A, can then be selectively etched in the developer MF319 to create an undercut and open up the hole to the substrate. Scale bar: 500 nm. (b) SEM image of Au seed particles in a hexagonal pattern. Scale bar: 500 nm.

Displacement Talbot lithography is a contact-free optical lithography technique for the creation of periodic patterns [115]. The interference pattern produced by collimated monochromatic light passing through the mask results in images of the periodic pattern of the mask [116]. These images are repeated periodically due to higher-order diffraction, the distance between them being the Talbot distance. Displacement Talbot lithography relies on an integration along the axis perpendicular to the mask by moving the substrate during the exposure, leading to a very stable reproduction of the periodic features of the mask. Similarly to nanoimprint lithography, a double-layer resist structure is used to enable lift-off after Au evaporation [116].

## 3.2 Nanowire Growth by MOVPE

Metal-organic vapor-phase epitaxy (MOVPE) is a technique for semiconductor epitaxy in which the constituent atoms are transported to the growth front in the gas phase. In contrast to molecular-beam epitaxy (MBE), the constituents are provided bound in precursor molecules, not as pure atoms. Since initial problems of MOVPE regarding purity as well as limitations hindering the realization of atomically sharp interfaces were overcome, MOVPE has become the main tool

for research and production of compound semiconductor heterostructure devices, such as LEDs, lasers and solar cells [117].

The precursor molecules used in MOVPE pyrolyze, i.e. break apart, when coming in contact with the heated substrate, and thereby liberate the desired constituent atom. The atoms will then diffuse on the surface of the substrate, and end up on a low-energy site in the semiconductor crystal [117]. When growing nanowires in the VLS growth mode, the Au seed particle acts as a reservoir for some of the constituent atoms, and growth is enhanced at the interface between Au particle and nanowire [118].

Important considerations concerning the choice of the precursor molecules are the kinetics of pyrolysis. The precursors have to be stable in storage at ambient temperature but pyrolyze readily when in contact with the heated substrate. Additionally, the reaction byproducts of pyrolysis should readily desorb from the semiconductor surface (often after reacting with each other), to prevent the incorporation of defects into the crystal [117].

Many different precursor molecules have been developed, which often differ in terms of bond strength and thus the dynamics and temperature of pyrolysis. For group II and III elements, metal-organic precursor molecules are most commonly used. For group V elements, metal-organic precursors are being developed, but group V hydrides remain the most commonly used option. In the work presented in this thesis, the group III precursors trimethylindium (TMIn), trimethylgallium (TMGa) and triethylgallium (TEGa) are used. The differences between using TMGa and TEGa stemming from their different pyrolysis characteristics are investigated in Paper II. Phosphine ( $\text{PH}_3$ ) is used as a group V precursor. For doping of III–V semiconductors, elements of group II and VI can be used as acceptors and donors, respectively. In this work, diethylzinc (DEZn) is used as an acceptor precursor, and hydrogen sulfide ( $\text{H}_2\text{S}$ ) and tetraethyltin (TESn) are used as donor precursors. The dopant atom Zn is in group IIB, S in group VI, and Sn in group IV. Group IV elements such as Sn can also be used as dopants, and will act as donors or acceptors depending on whether they preferentially replace a group III or group V atom in the III–V crystal structure.

Heterostructures can be grown in MOVPE by changing the precursors that are added to the carrier gas during growth. Ideally, atomically sharp interfaces are desired. In practice, that can be difficult to achieve due to limitations in the speed of switching and replacement of precursor gasses, as well as adsorption and desorption at reactor surfaces creating a reservoir effect. For VLS growth of nanowires, precursor and dopant atoms dissolved in the Au particle can create a further reservoir, which hinders the creation of atomically sharp interfaces.

Figure 3.2 (a) schematically shows the VLS growth process, using the example of InP growth by use of TMIIn and PH<sub>3</sub> precursors. Pyrolysis of the precursors can occur in the gas phase but is enhanced on the semiconductor as well as Au particle surface. The pyrolysis of TMIIn liberates methyl radicals, while hydrogen radicals are created from the PH<sub>3</sub>. Precursor molecules as well as the constituent atoms can migrate on the surface by random diffusion processes, leading to a certain probability that they will be transported to the Au particle, versus a probability that they will either desorb or incorporate into the semiconductor crystal in a planar growth process. Different materials have different diffusion coefficients on the semiconductor surface, which governs the effective precursor collection area of the Au particle. For example, the diffusion coefficient for In adatoms is significantly higher than for Ga adatoms [119, 120]. Thus, In atoms reach the Au particle to a large extent by means of surface diffusion, while Ga adatom delivery to the Au seed particle is predominantly due to other mechanisms, such as gas-phase diffusion of monomethylgallium (MMGa) [121].

Most group III elements including In readily dissolve in the Au particle at elevated temperatures to form an alloy [122]. Contrary to what the name of the VLS growth mode suggests, the Au alloy particle is not necessarily liquid – depending on the growth temperature and the concentration of group III elements in the Au particle, it can either be in liquid or solid state [118]. Diffusivities of the group III elements in both liquid and solid Au are very high [123], enabling nanowire growth in both cases [118, 122].

Group V atoms such as P, on the other hand, are not soluble in the Au particle at growth conditions [118]. Instead of being dissolved in the Au particle, they will diffuse to the growth front via the boundary of the Au particle and the NW, or along the grain boundaries of a solid Au particle [118].

### 3.3 Characterization of Nanowire Arrays

Characterization of the nanowire array properties was carried out using a number of techniques, which will be introduced below. They are used to characterize different properties of the nanowires, including the nanowire dimensions, the composition of ternary materials such as GaInP, and the doping profile.

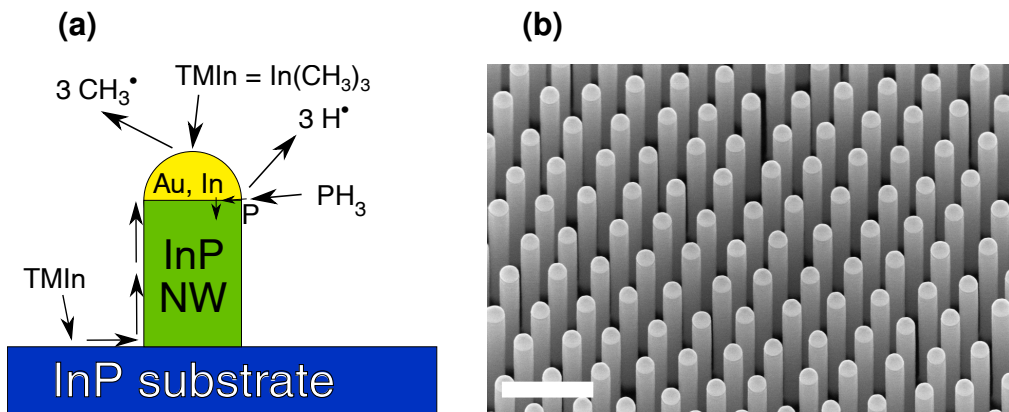


**Figure 3.2:** (a) Schematic illustration of the VLS growth process using trimethylindium (TMIIn) and phosphine ( $\text{PH}_3$ ) precursors and a Au seed particle for the growth of an InP nanowire. (b) SEM image of InP nanowires in a hexagonal pattern with a pitch of 500 nm. Au seed particles are visible at the tip of each nanowire. Scale bar: 1000 nm.

### 3.3.1 In-Situ Characterization by use of Optical Reflectometry

Optical reflectometry performed in-situ during nanowire growth is a powerful tool, making it possible to continuously evaluate the nanowire length during growth. This enables a high degree of control over nanowire growth, as the growth time of each nanowire segment can be adjusted to yield the desired segment length.

The used Laytec EpiR DA UV optical reflectometry setup measures the reflectance of the substrate in the 400–800 nm wavelength range in situ in the MOVPE reactor. As the length of the nanowires increases, interference of the reflections from the substrate and the Au particles at the nanowire tips occur, as shown in Figure 3.3 (a). As long as the length of the nanowires in the array is homogeneous, this produces an interference pattern, with local maxima/minima in reflectance due to constructive/destructive interference, respectively. Figure 3.3 (b) shows measurement results of a nanowire growth process, where the shift of local maxima and minima with increasing nanowire length is seen. At each point in time, the length of the nanowires can be inferred by comparing the measured nanowire array reflectance with optical modeling results [124].

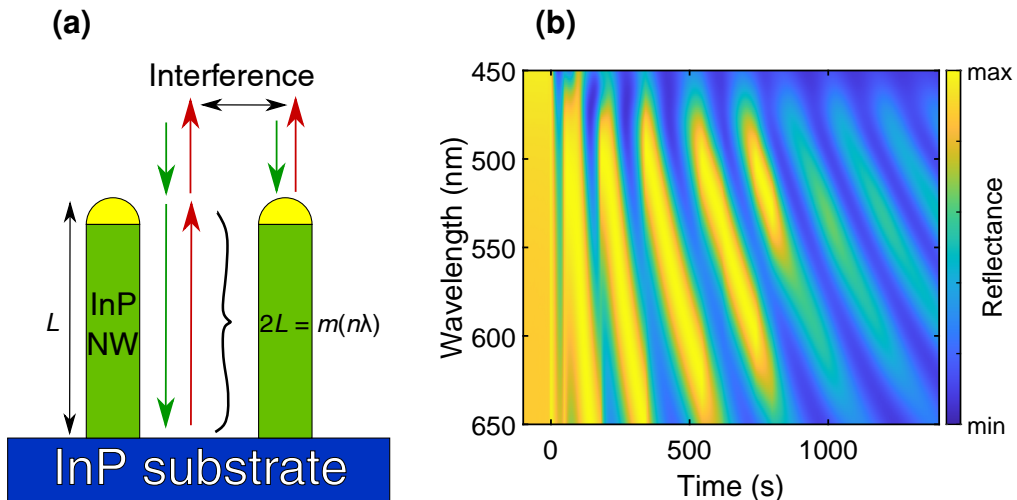


**Figure 3.3:** (a) Schematic illustration of the optical reflectometry measurement process during nanowire growth. The condition for constructive interference between the light reflected at the substrate and at the nanowire tips is indicated.  $L$  is the nanowire length,  $n$  the effective refractive index of the nanowire array,  $\lambda$  the wavelength of light and  $m$  an integer. (b) Results of an in-situ Laytec optical reflectometry measurement during nanowire growth. The shift of the local extrema towards longer wavelengths over time reflects the increasing length of the nanowires.

### 3.3.2 Scanning Electron Microscopy

One of the most versatile characterization tools in nanotechnology is the scanning electron microscope (SEM). A focused electron beam is scanned over the sample surface, where the high-energy incoming electrons interact with the atoms close to the spot position. The beam electrons can be elastically scattered back out of the sample as so-called backscattered electrons by interaction with nuclei. They can also interact with other electrons, transferring a fraction of their energy to an electron which is knocked out of the atom it was previously bound in and is called a secondary electron. The filling of the resulting orbital vacancy with an electron from a higher-energy orbital can lead to the emission of X-ray photons [125].

Backscattered electrons, secondary electrons as well as X-ray photons can be detected, and data is collected pixel by pixel and reconstructed to form an image. Both the backscattered electron and the secondary electron images give information about the local morphology and surface topography, while the detected X-rays can mainly be used to determine the materials composition of

the sample [125]. For the characterization of nanowires, SEM with a secondary electron detector was used to determine the nanowire morphology, measure the length and diameter, and check for defective or missing nanowires in an array. The SEM images can also give some limited insight into the nanowire crystal phase and composition.

### 3.3.3 Electron-Beam Induced Current Measurements

As discussed in section 2.1, the working principle of most solar cells, including the III–V nanowire solar cells discussed in this work, is based on the separation of photon-generated electron–hole pairs in the electric field on a p–n junction. In order to optimize device functionality, good control and evaluation of the doping level is desired. However, for nanowires, the standard technique of doping evaluation by Hall effect measurements is much more challenging to implement compared to planar layers. Both the fabrication of the Hall structure and the measurement on a single nanowire is challenging, as electron-beam lithography is needed to define contacts at the sides of a nanowire [126–128]. Alternative methods of nanowire doping evaluation include optical methods based on photoluminescence measurements that are easier to implement, but more prone to possible systematic errors [100, 128–131].

A different approach lies in the characterization of the doping heterostructure by electron-beam induced current (EBIC) measurements. While EBIC is not suitable for obtaining an absolute value of dopant or charge carrier concentrations, it can help in understanding the functionality of the p–n junction device by characterizing the junction location.

EBIC is performed inside an SEM which is equipped with a nanoprobe for contacting a single nanowire. The piezo-controlled conductive probe is used to make an electrical contact to the Au particle at the nanowire tip. This enables electrical measurements of the contacted single nanowire, both in dark conditions and under illumination [132]. For performing an EBIC measurement, the electron beam is scanned across the nanowire, just like it is when recording an SEM image. Instead of recording the number of emitted secondary electrons, the current through the nanowire is measured for each position of the scanning electron beam, and reconstructed into an image.

When the focused electron beam interacts with the semiconductor material, it creates electron/hole pairs within the excitation volume, i.e. within a certain distance from where the electron beam hits the sample. If the excitation happens within the depletion region of the p–n junction, the charge carriers are separated

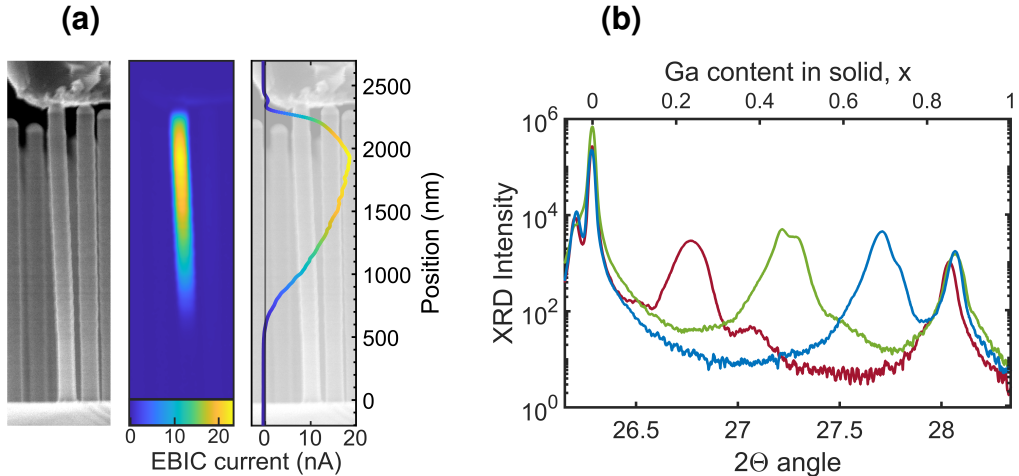


**Figure 3.4:** (a) Results of an EBIC measurement. Left panel: SEM image of the measured nanowire. Center panel: color-coded image of the EBIC current as a function of the electron beam position. Right panel: EBIC current as a function of axial position, averaged over the width of the nanowire. The SEM image is overlaid for reference. (b) Normalized X-ray diffraction intensity as a function of  $2\Theta$  measured on three different GaInP/InP tandem junction nanowire arrays standing on InP substrates. The upper x-axis shows the corresponding Ga content  $x$  for  $\text{Ga}_x\text{In}_{1-x}\text{P}$ , calculated by use of Vegard's law. The three arrays of GaInP/InP tandem junction nanowires have a different Ga content of the GaInP subcell, creating peaks at different  $2\Theta$  angles. The samples share the InP peak and a peak at high Ga content (around 85 %) which corresponds to the GaInP segment of the Esaki tunnel junction.

by the built-in electric field of the p–n junction, contributing to a current through the nanowire. This effect can be used to map the location of the depletion region within the nanowire. In the example shown in Figure 3.4 (a), an InP p–i–n junction nanowire, the depletion region spans the intrinsic and a large fraction of the n-type region.

### 3.3.4 X-ray Diffraction

X-ray diffraction (XRD) measurements are a standard method for measuring the lattice constant in crystalline materials. Constructive interference of reflected X-ray radiation from each lattice plane occurs when Bragg's law  $2d \sin \Theta = n\lambda$  is satisfied [28].  $d$  denotes the distance between successive lattice planes,  $\Theta$  is the angle between the plane and the incoming X-ray beam, and  $\lambda$  is the X-ray

wavelength. The measurement is done by scanning over the  $\Theta$  angle, and is reported as X-ray intensity as a function of  $2\Theta$ .

For III–V semiconductor nanowire arrays, the measurement of the lattice constant by use of XRD can yield information about the composition of the material. The lattice constant of a ternary material can, to first approximation, be calculated as the weighted mean of the binary lattice constants, which is known as Vegard’s law. For example, an XRD measurement of the GaInP ternary along the [111] crystallographic direction will result in a peak located between  $2\Theta = 26.28^\circ$  for InP ( $a = 5.870 \text{ \AA}$ ) and  $2\Theta = 28.34^\circ$  for pure GaP ( $a = 5.451 \text{ \AA}$ ) [133]. An example of XRD measurements on GaInP/InP tandem junction nanowires is shown in Figure 3.4 (b), showing an InP peak, and two peaks of GaInP with different compositions for each of the three measured samples. These peaks stem from different segments of the GaInP/InP tandem junction nanowires – the GaInP segment with a high Ga content is part of the Esaki tunnel junction, and the other GaInP peak stems from the GaInP sub-cell.

### 3.3.5 Photoluminescence and Photoluminescence Mapping

Photoluminescence (PL) measurements are performed by illuminating a sample and measuring the light emitted by it. The excitation is performed using a laser which provides focused light with a photon energy above the band gap of the investigated semiconductor material. After the optical excitation of electron–hole pairs and the thermalization of the charge carriers, radiative recombination can lead to the emission of light, which is collected through an objective and detected by use of a spectrometer. The photon energy of the emitted light will be determined by the band gap of the material, the presence of radiative defect states near the band edges, the intensity of excitation and resulting state-filling, as well as the temperature [134]. Apart from radiative recombination, charge carriers can also be trapped and recombine non-radiatively, through the Shockley–Read–Hall (SRH) recombination mechanism or via surface recombination [134].

PL characterization of nanowires can be performed on individual nanowires broken off from the substrate and transferred to a different substrate, often a Si wafer, for a low background and the highest possible measurement accuracy [135–137]. It is also possible to perform PL measurements on nanowires standing on the native substrate in sufficiently dense arrays, as the nanowires absorb the short wavelength excitation light efficiently [138].

By focusing the excitation on a small area, the collected PL contains information about that local position on the sample. In PL mapping, the sample is moved in small steps in order to create a map, which contains the PL information as a function of the position on the sample.

### 3.3.6 Time-Resolved Photoluminescence

Time-resolved photoluminescence (TRPL) is used to gain an understanding of the temporal dynamics of the processes that charge carriers undergo after excitation. In particular, it is used to measure the carrier lifetimes in the material, which can give an indication of the materials quality. In particular, a high concentration of defect states can lead to short carrier lifetimes due to higher rates of nonradiative recombination, which can be quantified using TRPL. Due to their geometry, nanowires inevitably have a large surface-to-volume ratio. An increased number of defects at the nanowire surface can therefore dominate the nonradiative recombination rate of the nanowire, which makes surface passivation essential for achieving a high performance in nanowire optoelectronic devices [139–141].

The basic working principle of TRPL is the use of a short laser pulse to generate electron–hole pairs, followed by the time-resolved detection of the PL signal emitted from the sample. The detection can take place using time-correlated single photon counting, or a streak camera that provides both spectral and temporal resolution, but at the cost of a lower quantum efficiency and higher complexity of the measurement setup [134, 142].

# 4 Processing and Characterization of Nanowire Solar Cells

## 4.1 Processing of Nanowire Solar Cells

The processing of nanowire solar cells comprises several steps, leading from an array of free-standing nanowires to a number of photovoltaic devices, each connecting millions of nanowires in parallel. The starting point for the devices described in the following are p-i-n doped InP nanowires, which matches the structure used in Paper I. The p/n stands for p-doped/n-doped segments, respectively, and i denotes a compensation doped segment, which is intended to behave like intrinsic material [141, 143]. More complex tandem junction GaInP/InP nanowires can be processed into devices following the same procedure.

The working principle p-i-n photovoltaic nanowires is equivalent to that of planar p-n-junction based solar cells, which is discussed in section 2.1. The role of the additional intrinsic middle segment is to create an extended depletion region, leading to the presence of the built-in electric field and an efficient separation of electron-hole pairs along most of the nanowire [143]. Just like in a p-n-junction, the built-in electric field of the p-i-n-junction acts to separate photogenerated charge carriers, and transports electrons to the n-side (top) and holes to the p-side (bottom) of the nanowires, creating a current [144]. The charge carriers are finally collected through the front and back electrodes, with the additional requirement for the front electrode to have good transparency for the incoming solar radiation. Figure 4.1 (a) shows a schematic of the processing steps involved in contacting the nanowires, and Figure 4.1 (b) shows an SEM image of the fully processed nanowire array.

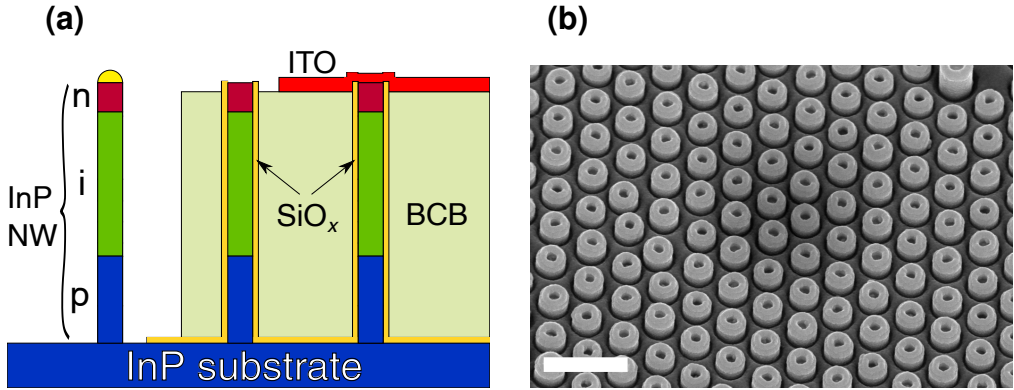


**Figure 4.1:** (a) Illustration of the steps involved in the processing of nanowire arrays into solar cells. The leftmost nanowire is shown as-grown. The center nanowire is shown coated with  $\text{SiO}_x$  and planarized with BCB. An opening has been etched into the  $\text{SiO}_x$  using RIE, and the Au particle has been removed by wet chemical etching. The rightmost nanowire is shown following the deposition of 150 nm thick ITO as a transparent top contact. (b) SEM image of a vertically processed nanowire array, corresponding to the rightmost nanowire in the illustration in panel (a). Scale bar: 1000 nm.

The first processing step is to protect the nanowire sidewalls using silicon oxide ( $\text{SiO}_x$ ), which is deposited using atomic layer deposition (ALD) with the precursors tris(tert-butoxy)silanol (TTBS) and trimethylaluminum (TMAI) [143]. The resulting oxide is termed  $\text{SiO}_x$  (as opposed to  $\text{SiO}_2$ ) because it is not necessarily stoichiometric, and it furthermore contains a low amount of Al ( $\approx 0.6$  at.%) [145]. A high concentration of defect states can be located at the sidewalls of the nanowires, leading to increased nonradiative recombination. The role of the  $\text{SiO}_x$  is therefore to passivate and protect the NW sidewalls from unwanted interaction with chemicals used during the processing [141].

Next, a planarization step is performed by spin-coating bisbenzocyclobutene (BCB, product name Cyclotene 3022-46), and etching it back using reactive ion etching (RIE) to expose the nanowire tips. RIE is also used to create an opening in the  $\text{SiO}_x$  at the NW tips, such that it will be possible to contact them electrically at the top. To obtain a top contact with good electrical conductivity, the Au seed particles are etched, and 150 nm thick indium tin oxide (ITO) is sputtered as a top electrode. To create several photovoltaic devices with a well-defined area on the sample, three photolithography steps are used, as illustrated in Figure 4.2 (a). The first lithography step takes place before the deposition of ITO. To define a frame around the active device area, S1828 photoresist is applied and hard-baked. After ITO sputtering, the ITO between devices is

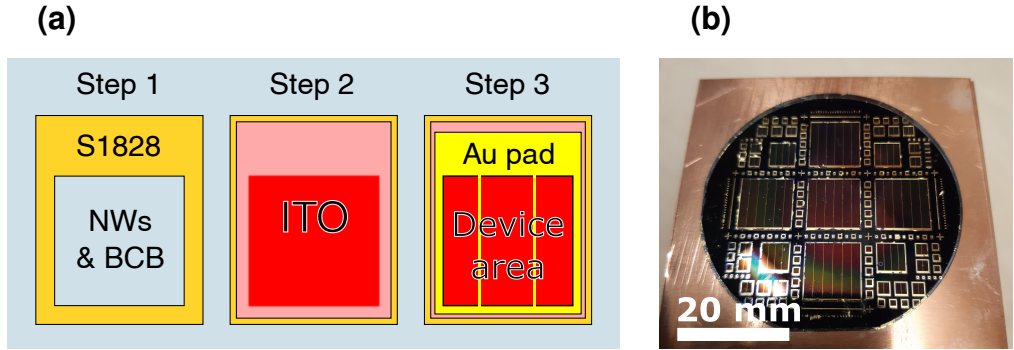


**Figure 4.2:** (a) Definition of solar cell devices by use of photolithography. Step 1: The (hard-baked) S1828 frame defines the device area, in which the nanowire tips are exposed. BCB for planarization is present on the entire sample. Step 2: ITO is sputtered onto the sample, and then selectively etched between the devices. An etch mask of S1813 is used to protect the ITO from the HCl-based etchant. In the active area of the device, where the nanowire tips are exposed, the ITO acts as a top contact. Step 3: A bus bar of Au is evaporated around the active area of the device for the collection of the generated current. The bus bar is made wider on one side, where it acts as a contact pad for contacting with a probe or by wire bonding. For the largest devices, fingers extend over the device area to minimize resistive losses in the conductive ITO layer. A lift-off procedure using the negative photoresist ma-N 490 is used for the Au bus bar definition. (b) Photograph of a processed 2-inch InP nanowire solar cell sample, with devices ranging in size between  $200 \times 200 \mu\text{m}$  and  $10 \times 10 \text{mm}$ . The back side of the wafer is connected to the copper plate using conductive silver paste.

etched using a photoresist etch mask, in order to electrically isolate the devices from each other. Finally, to define Au contact pads, an evaporation and lift-off procedure with a negative photoresist is used.

The Au pad of a device can then be contacted with a probe to measure the photovoltaic device performance. As the nanowires are standing on a conductive substrate, the contact to the bottom of the nanowires can be made at the back side of the substrate, by evaporating Ti/Zn/Au and mounting the substrate on a copper plate by use of conductive silver paste<sup>1</sup>. This means that the back contact is made to all of the nanowires on a sample simultaneously, while only the nanowires in the active area of a selected device are contacted from the top via the respective Au contact pad.

<sup>1</sup>The Zn layer helps to create an ohmic contact to the p-type substrate. When processing nanowire arrays standing on an n-type substrate, only Ti/Au is used.

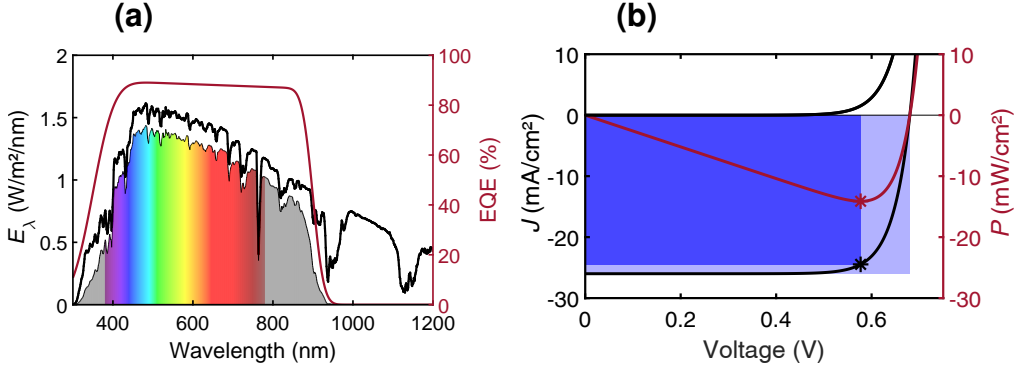


**Figure 4.3:** (a) Schematic plot of a possible EQE curve for an InP solar cell (red curve). The black curve shows the spectral power density of the AM1.5G solar spectrum. The shaded area marks the photons that contribute towards the short-circuit current, obtained by multiplying the solar spectrum with the EQE. (b) Schematic drawing of  $J$ - $V$  curves of an InP solar cell in the dark and under illumination (black lines). The red line shows the power density as a function of voltage. The area spanned by  $J_{SC}$  and  $V_{OC}$  is highlighted in light blue, while the area spanned by the operating voltage and current density at the maximum power point (MPP) is marked in dark blue.

The size of the processed nanowire photovoltaic devices is defined by the used UV lithography masks and can be varied in a wide range. An image of processed nanowire solar cells on a full 2-inch wafer is shown in Figure 4.2 (b).

## 4.2 Characterization of Nanowire Solar Cells

To characterize nanowire solar cells, the well-established methods of solar cell characterization used for planar solar cells can be applied.

### 4.2.1 External Quantum Efficiency

The basic operating principle of a solar cell is, as described in section 2.1, the separation of light-generated electron-hole pairs by the built-in electric field of a p-n junction. The external quantum efficiency (EQE) of a solar cell measures the ratio of the current – measured as the number of electrons – to the number of incoming photons under short-circuit conditions. The EQE depends on the wavelength of the incoming light and is reported as a function of wavelength.

Ideally, each incoming photon with an energy  $\hbar\omega > E_g$  can create one electron–hole pair which contributes to the current, which would represent an EQE of 100 % for that wavelength. In reality, a number of factors limit the EQE, such as the reflection of incoming light, recombination of charge carriers, and incomplete light absorption. A schematic depiction of the EQE of an InP nanowire solar cell is seen in Figure 4.3 (a). Low-energy photons with a wavelength above 950 nm, corresponding to an energy below the InP band gap, are not absorbed. For short wavelengths below 400 nm, the EQE is reduced because of absorption in the ITO front contact, reflection, as well as strong light absorption near the top contact of the nanowires, which leads to enhanced recombination.

### 4.2.2 Current Density–Voltage Characteristics

To generate power, a solar cell is operated under forward bias conditions. The total current density in the p–n junction is described by the diode equation

$$J = J_0 \left( \exp \left( \frac{eV}{nk_B T} \right) - 1 \right) - J_{\text{ph}} \quad (4.1)$$

where  $J_0$  denotes the dark saturation current density,  $e$  is the elemental charge,  $V$  the voltage,  $k_B T$  the thermal energy, and  $n$  the diode ideality factor [146]. Under illumination, a photocurrent  $J_{\text{ph}}$  is generated in the reverse direction of the diode.

Figure 4.3 (b) shows schematic current density–voltage ( $J$ – $V$ ) curves. The state in which  $U = 0$  V is called short-circuit, characterized by the short-circuit current density  $J_{\text{SC}}$ . The open-circuit voltage  $V_{\text{OC}}$  is similarly defined as the voltage under open-circuit conditions, i.e.  $J = 0$  mA/cm<sup>2</sup>. While  $J_{\text{SC}}$  and  $V_{\text{OC}}$  are important parameters of a solar cell, no power is generated under both short-circuit and open-circuit conditions. Instead, the output power density  $J \cdot V$  is largest when both the current density  $J$  and the voltage  $V$  are high, at a point called the maximum power point MPP. As both  $J_{\text{MPP}} < J_{\text{SC}}$  and  $V_{\text{MPP}} < V_{\text{OC}}$ , the maximum power density  $P_{\text{max}} = J_{\text{MPP}} \cdot V_{\text{MPP}} = J_{\text{SC}} \cdot V_{\text{OC}} \cdot \text{FF}$  will be smaller than  $J_{\text{SC}} \cdot V_{\text{OC}}$ , where the fill factor FF is defined as the fraction of the maximum output power divided by  $J_{\text{SC}} \cdot V_{\text{OC}}$ . Graphically, this can be understood as the area fraction of the rectangle spanned by the origin and the maximum power point MPP to the area of the rectangle defined by  $J_{\text{SC}}$  and  $V_{\text{OC}}$ , as illustrated by the shaded area in Figure 4.3 (b).

### 4.2.3 Photoluminescence and Light-Beam Induced Current Mapping

Apart from measurements on single nanowires and nanowire arrays (discussed in section 3.3.5), photoluminescence (PL) measurements can also be recorded on fully processed solar cell devices. PL mapping measurements in particular can be used to obtain spatially resolved information indicating local defects on the solar cell. The possibility to apply a voltage to the solar cell and measure the PL intensity as a function of applied voltage adds further characterization options [147, 148].

The contacts to the solar cell can also be used to measure the photocurrent generated by the illuminating laser spot, in a so-called light-beam induced current (LBIC) measurement. To achieve this, a laser beam is scanned over the sample surface, and the induced photocurrent is measured for each position of the laser beam [149–151]. LBIC mapping and PL mapping measurements can be performed in the same measurement setup in order to enable an analysis correlating the two recorded maps, as done in Paper I.

### 4.2.4 Electroluminescence Imaging

The process of light emission by radiative electron–hole recombination is complementary to the process of light absorption and generation of electron–hole pairs. This means that a material with a high photovoltaic quantum efficiency will in theory also be a good light emitter [152]. In practice, solar cells and light-emitting diodes (LEDs) are optimized using different objectives and thus differ substantially from each other. However, the basic notion that a solar cell can also work as an LED remains valid, and electroluminescence (EL) can be used to characterize solar cells [153]. To obtain an EL signal, the solar cell is operated under high forward bias, where electrons and holes are injected into the p–n junction and recombine. Imaging the EL emission of a solar cell, often at several different bias voltages, can be used as a rapid way of extracting spatially resolved information about the solar cell performance [154–156]. Compared to the sequential processes of PL and LBIC mapping, an EL emission image can be recorded in a single exposure using a microscope objective and a CCD detector.

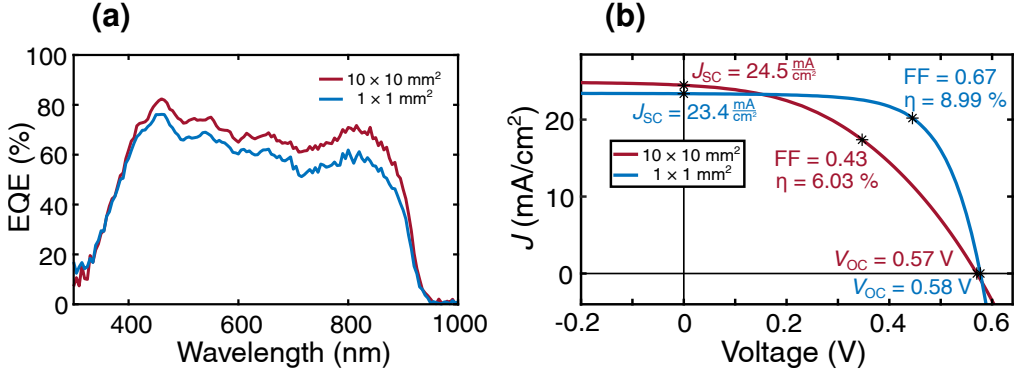


**Figure 4.4:** Characterization results on a large area  $10 \times 10 \text{ mm}^2$  device compared to a smaller,  $1 \times 1 \text{ mm}^2$  sized device on the same sample. (a) External quantum efficiency. (b)  $J$ – $V$  characteristics. Values of  $V_{\text{OC}}$ ,  $J_{\text{SC}}$ , fill factor FF and solar conversion efficiency  $\eta$  are indicated. Figures adapted from Paper I.

### 4.3 Large Area Nanowire Solar Cells – Results of Paper I

Nanowire solar cells are an emerging technology, and the research has so far focused on improving the performance of small, mm- or sub-mm-scale devices [75]. In Paper I, we explore the effects of increasing the device size to  $10 \times 10 \text{ mm}^2$ , performing the nanowire growth and device processing on a full 2-inch wafer. The objective of this study was to bring nanowire solar cells closer to commercial viability in niche markets, such as space applications [87, 88]. A photograph of the resulting vertically processed 2-inch wafer is seen in Figure 4.2 (b), featuring devices ranging between  $200 \times 200 \mu\text{m}^2$  to  $10 \times 10 \text{ mm}^2$  in size.

Working on a full 2-inch wafer means that approximately 9 billion vertically standing nanowires are grown at the same time. As shown in previous work, wafer patterning and nanowire synthesis can be performed with good homogeneity at this size scale [157]. The largest devices defined during processing, with an area of  $10 \times 10 \text{ mm}^2$ , connect 460 million nanowires in parallel. On these large devices, defects from patterning, nanowire growth and processing are present in every device. Paper I explores the extent to which these defects impact device performance using PL and LBIC mapping, concluding that the defects present on the investigated device prevent current generation locally, but have a limited impact on the total performance of the device.

Figure 4.4 shows EQE and IV measurements of a processed large area nanowire solar cell, as well as the performance of a smaller device on the same sample, for comparison. Importantly, the EQE and short-circuit current density  $J_{SC}$  of the large area nanowire solar cell are on par with the smaller device, confirming the successful parallel contacting of most nanowires constituting the  $10 \times 10 \text{ mm}^2$  nanowire solar cell. However, the fill factor  $FF$  in the  $J-V$  curve of the large area device is significantly lower, limiting the overall device efficiency. By performing EL measurements, the series resistance of the ITO transparent top contact is found to be the cause of the reduced fill factor.

## 4.4 Peel-Off of Nanowire Arrays

Removing the nanowires from the substrate using a polymer film promises a number of advantages. It makes the re-use of the growth substrate possible, as well as enabling the fabrication of flexible solar cells based on nanowire arrays embedded in a thin polymer film. Additionally, it is possible to make the resulting nanowire solar cells semi-transparent. Usually, a complete absorption of the incoming sunlight is desired, to attain a maximum possible efficiency. However, semi-transparent solar cells open up for new applications where opaque solar cells cannot be used [158]. Most strikingly, by integrating semi-transparent solar cells into windows, solar power generation could be combined with a reasonable transparency of the window. Applications for this approach include energy-efficient office buildings as well as agricultural applications such as integrating solar cells into greenhouses [159, 160].

Transparency of a solar cell can be achieved in different ways, which all come at the cost of reduced light absorption and thus efficiency. One option is to make the absorbing material thin enough to enable a fraction of the above-band gap light to pass through the solar cell [158]. Geometric structuring can also be used to create adjacent areas where light is absorbed/transmitted. If these areas are spaced close enough to each other, an overall semi-transparent impression can be achieved [158].

Furthermore, by using a semiconductor material with a high band gap, the portion of visible light that has a photon energy below the band gap can be increased, also contributing to better transparency [161]. However, this approach suffers from the problem that only a very low fraction of the energy contained in sunlight is found in the ultraviolet spectral region with high photon energy, as seen from the AM1.5G solar spectrum in Figure 4.5 (a). Thus, a solar cell

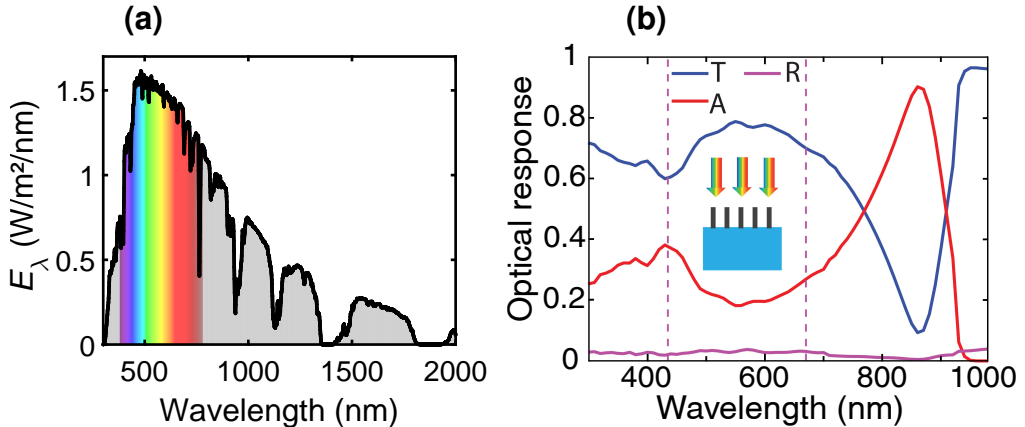


**Figure 4.5:** (a) Spectral power density of the AM1.5G solar spectrum. (b) Simulated absorption (A), transmission (T) and reflectance (R) of a free-standing InP nanowire array for transparent solar cell applications. The visible region (420 – 680 nm) is indicated. Figure adapted from Paper II.

achieving transparency by means of a high band gap energy will have a very small number of photons available for absorption.

In contrast, a large portion of the solar energy is found in the infrared spectral parts of the spectrum. However, absorbing parts of the infrared light requires a low band gap – which in turn leads to strong absorption also in the visible region. In Paper II, the authors present a strategy to obtain InP nanowire arrays with good transparency to visible light and simultaneous absorption in the near-infrared.

## 4.5 Peel-Off of Semi-Transparent Nanowire Arrays – Results of Paper II

The main idea of Paper II is utilizing the strong absorption of light coupling into the fundamental optical mode of nanowires. By tuning the nanowire diameter, the wavelength of the absorption peak due to optical resonance can be adjusted [20, 162]. For nanowire array solar cells it is usually tuned to generate the strongest possible absorption of light around the maximum of the solar spectrum. In Paper II, in contrast, the InP nanowire diameter of 170 nm is chosen to have maximum absorption around 850 nm, outside of the visible spectrum. By spacing the nanowires in a sparse array with a pitch of 1000 nm, a good

transmission of visible light is achieved, while maintaining strong absorption of the near-infrared light around the optical resonance peak. This is demonstrated in Figure 4.5 (b), which shows the simulated absorption, transmission, and reflection of light by such an InP nanowire array.

Experimentally, Paper II presents the results of peeling off an array of InP nanowires by embedding them into a polydimethylsiloxane (PDMS) film, curing the PDMS, and mechanically removing the PDMS film including the embedded nanowires from the substrate. Optical transmission and reflection measurements have verified the simulation results, showing good transmission of visible light as well as strong absorption in the near-infrared.

# 5 GaInP/InP Tandem Junction Nanowire Solar Cells

## 5.1 Working Principles of Tandem Junction Solar Cells

The idea of tandem junction solar cells is to use separate sub-cells for the absorption of different parts of the solar spectrum. By absorbing high-energy photons in a high band gap semiconductor and lower energy photons in a low band gap semiconductor, thermalization losses are minimized. Figure 5.1 illustrates this

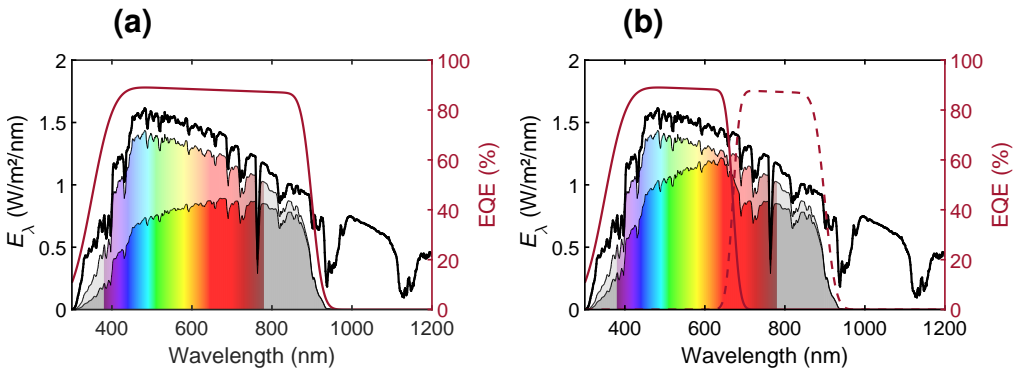


**Figure 5.1:** Spectral power density of the AM1.5G solar spectrum (black curve) and schematic EQE curves (red) for **(a)** a single junction InP solar cell, and **(b)** a tandem junction GaInP/InP solar cell. In both panels, the lightly shaded area shows the amount of photons that are absorbed and contribute to the short circuit current density  $J_{SC}$ . The darker, more intensely colored area represents the fraction of energy that can be extracted from these photons by the solar cell, where thermalization losses have been subtracted.

by highlighting the fraction of the solar spectrum which can be converted to electrical power by a single junction and a tandem junction solar cell, respectively. In theory, the higher the number of junctions made from different band gap materials, the smaller the wavelength range absorbed by each segment, and thermalization losses are reduced further for each added junction [163].

The standard concept for splitting the solar spectrum into wavelength ranges absorbed by different sub-cells is to stack the sub-cells on top of each other. In this way, the below-band gap photons not absorbed by the top junction semiconductor are available for the next junction. In principle, each of the sub-cells could be contacted as an individual solar cell and operate independently from the other sub-cells. However, the need for a transparent conducting layer for each intermediate contact complicates this setup significantly [163, 164]. Therefore, a 2-terminal configuration with just one top and one back contact is most common, where the sub-cells are connected in series. In this case, the voltages of the sub-cells are added, and the current must be the same in each subcell. The sub-cell with the lowest generated current thus acts current-limiting for the entire device. To achieve maximum performance, the sub-cells need to be current-matched, which can be achieved by tuning the respective band gap [165].

### 5.1.1 Esaki Tunnel Diode

To connect the sub-cells in a tandem junction solar cell, an ohmic connection should be made between the n-type and p-type segment of the respective sub-cells. To achieve this, an Esaki tunnel junction is used. The Esaki tunnel junction is formed between degenerately doped p- and n-type regions of a p–n junction if the depletion region is short enough to allow tunneling from one side of the p–n junction to the other, as visualized by the red arrow in the band diagram shown in Figure 5.2 (a). Electrons from the conduction band on the n-doped side can tunnel into the empty states in the valence band on the p-side. In the other direction, electrons from the valence band on the p-side can tunnel into empty states in the conduction band on the n-side. At thermal equilibrium, i.e.  $U = 0$ , these processes are in balance, and the net current is 0. Under forward bias, the tunneling of electrons from n-side to p-side increases, leading to a forward current, as seen in the red region marked in the schematic  $J$ – $V$  curve in Figure 5.2 (b). As the forward bias increases, fewer electrons will be able to tunnel through the diode, because fewer of the occupied energy levels on the n-side are aligned with the empty levels on the p-side, decreasing the current and leading to the phenomenon of negative differential

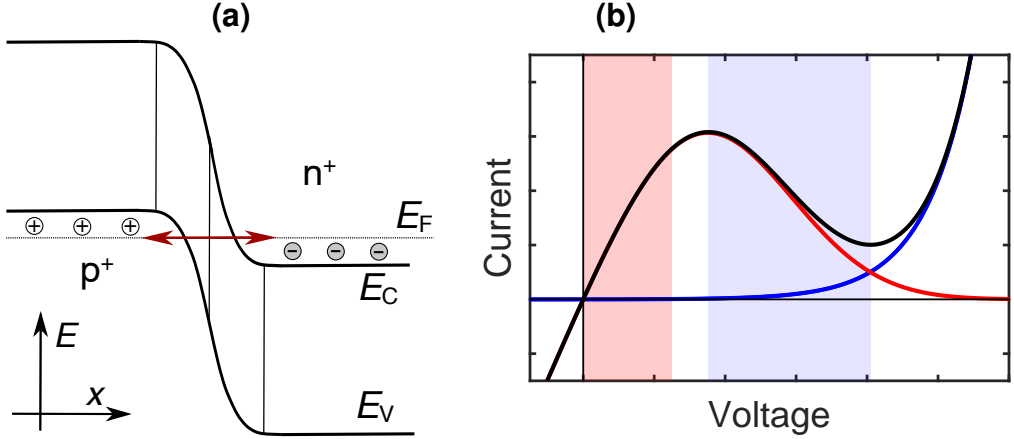


**Figure 5.2:** (a) Band structure of an Esaki tunnel diode, realized by degenerate doping on both sides of the junction. The red arrow indicates the tunneling of electrons through the junction, which dominates the current at negative bias and low forward bias conditions. (b) Schematic  $J-V$  curve of an Esaki tunnel diode. The red curve shows the tunneling current, the blue curve the diffusion current, and the black curve the total current. The blue area highlights the region with a negative differential resistance. The red area shows the operating region of the Esaki tunnel junction in a tandem junction solar cell.

resistance in the region marked light blue. At higher forward bias, the Esaki junction behaves as a normal p-n junction, as tunneling is not possible under those conditions. In a tandem junction solar cell, the Esaki tunnel junction is operated under low forward bias conditions (the red region in Figure 5.2), where its  $J-V$  characteristics are approximately ohmic. It thus acts just like a resistor connected in series with the sub-cells.

### 5.1.2 Voltage Addition in Tandem Junction Solar Cells

To illustrate the structure of a tandem junction solar cell, we can consider the case of a GaInP/InP nanowire solar cell, as presented in Paper IV. The full structure of the GaInP/InP tandem junction nanowire solar cell is shown in Figure 5.3. The band structure shows the two p-n junctions connected in series with the Esaki tunnel diode between them. The incoming light is partially absorbed in the high band gap GaInP top junction, with high-energy photons being absorbed and below band gap energy photons transmitted. These can then be absorbed in the lower band gap InP bottom junction. The current generated in the two subcells has to be equal due to the fact that they are

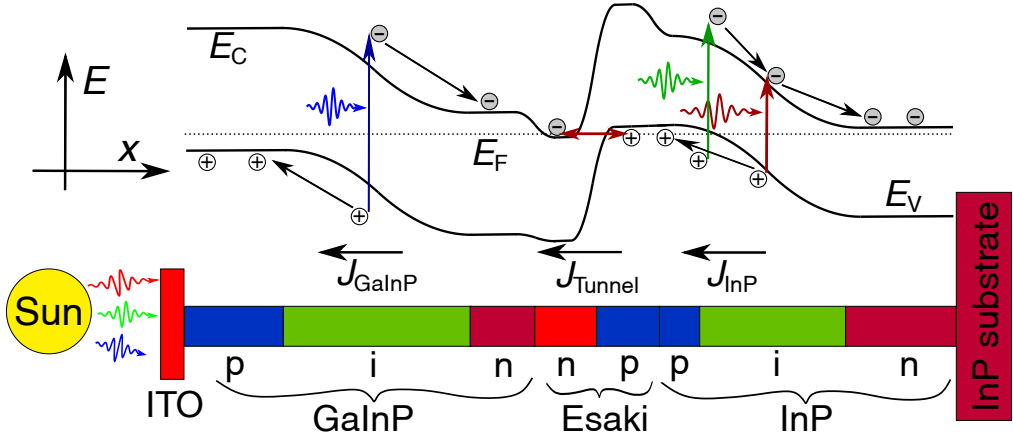


**Figure 5.3:** Band diagram of a tandem junction GaInP/InP nanowire solar cell showing the axial direction of the nanowires as x-axis and energy as y-axis, together with a schematic drawing of the nanowire. High energy photons are absorbed in the GaInP top cell, below band gap photons are transmitted through it. They can then be absorbed in the InP bottom cell which has a lower band gap. The sub-cells are connected by an Esaki tunnel junction. Figure reprinted from Paper IV.

connected in series. The Esaki tunnel junction will be in a slightly forward biased state in which the current through it matches the photocurrent of the subcells. We can summarize that  $J_{tot} = J_{GaInP} = J_{Tunnel} = J_{InP}$ , which is a reverse (photo-)current for the GaInP and InP subcells, but a forward current for the Esaki tunnel junction which is oriented in the opposite direction. The total voltage will be the sum of all voltages, which can be expressed as  $U_{tot} = U_{GaInP} - U_{Esaki} + U_{InP}$ , where all voltages are positive with respect to the direction of the respective junction. Figure 5.4 illustrates the voltage addition of the subcells and the Esaki tunnel junction. The voltage of the Esaki diode is subtracted because of the opposite direction of the Esaki tunnel junction.

## 5.2 MOVPE Growth of GaInP – Results of Paper III

GaInP is an attractive top junction material for tandem junction nanowire solar cells [162]. Paper III focuses on the growth and characterization of GaInP nanowire segments by use of two different Ga precursors, trimethylgallium (TMGa) and triethylgallium (TEGa). The aim of the paper is to understand which of these two precursors is most suitable for the growth of the GaInP segment of tandem junction solar cells. In order to have similar conditions as during the

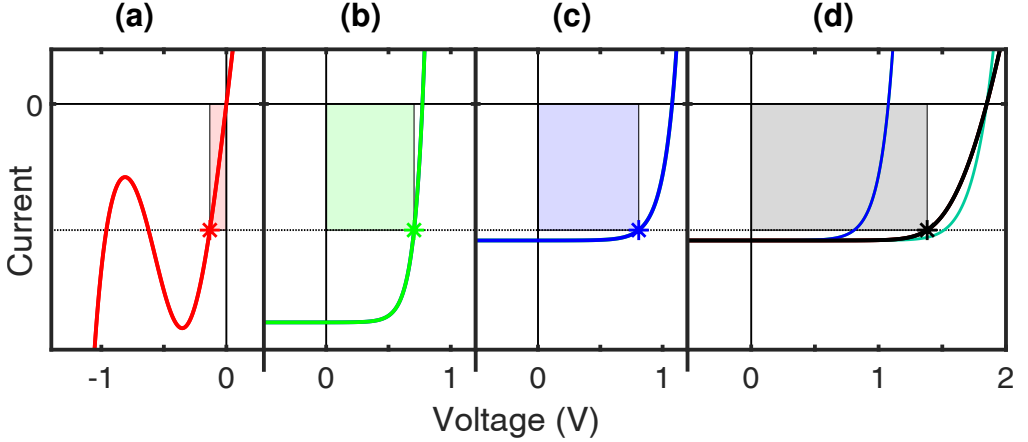


**Figure 5.4:**  $J$ - $V$  curves of the Esaki tunnel junction (panel (a)) as well as the sub-cells (panels (b) and (c)) in a tandem junction solar cell. In panel (d), the voltages of the subcells at equal current density are added up. The cyan curve represents the voltage addition of the two sub-cells, and the black curve represents the full structure including the voltage drop over the Esaki tunnel junction. In this case, the subcell in panel (c), plotted with a blue line, is current limiting. In each panel, the shaded area represents the generated/dissipated power. Both subcells generate power, while the Esaki tunnel junction dissipates a small amount of power.

growth of the tandem junction nanowires (with a structure as shown in Figure 5.3), the GaInP nanowire segment was grown on top of an undoped InP segment, as shown in Figure 5.5.

It is known that TEGa has favorable pyrolysis properties compared to TMGa due to a lower homogeneous pyrolysis temperature, resulting in a reduced consumption of the precursor material [166]. The results of Paper III confirm the favorable growth dynamics of GaInP nanowire segments grown using TEGa, including the more efficient utilization of the precursor.

It has been shown that the addition of the dopant precursor diethylzinc (DEZn) can strongly affect the TMGa pyrolysis and, by extension, the composition of the GaInP [167]. No similar investigation had been performed for the case of GaInP nanowire segments grown by use of the TEGa precursor. To address this question, Paper III investigates the effects of doping with hydrogen sulfide ( $H_2S$ ), tetraethyltin (TESn) and DEZn on the GaInP composition and crystal structure. No pronounced influence of the dopant precursors on the GaInP composition is found when using the TEGa precursor, in contrast to the case of using TMGa, for which the strong effect of DEZn on the GaInP composition is confirmed [167]. Thus, the use of the TEGa precursor is favorable for the

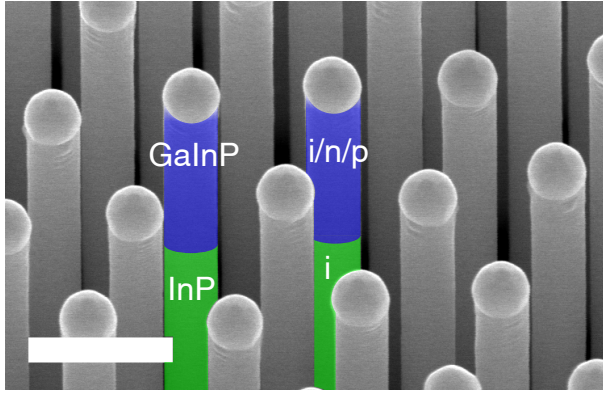


**Figure 5.5:** SEM image of GaInP/InP nanowires used for the GaInP growth study in Paper III. As indicated, the GaInP top segment doping is varied between samples, while the InP bottom segment is not doped. Scale bar: 500 nm.

growth of GaInP nanowires with doping heterostructures, such as the n-i-p doped GaInP subcells for tandem junction nanowire solar cells.

The properties of GaInP nanowires have previously only been studied for nanowires grown using the more common precursor TMGa [128, 168–170]. For future use of the alternative Ga precursor TEGa it is important to know if the GaInP nanowires grown by use of this precursor have a comparable materials quality.

In Paper III, time-resolved photoluminescence (TRPL) lifetimes are used as a proxy for the assessment of the GaInP materials quality. Figure 5.6 shows a comparison of the TRPL decay for GaInP nanowires grown by use of either TMGa or TEGa. GaInP nanowires with different compositions were measured, and a general trend of shorter lifetimes with increasing Ga content was observed, which is in line with previous results [171]. Comparing the nanowire arrays grown by different precursors but with similar Ga content, somewhat longer lifetimes are observed for the nanowires grown by use of TEGa. This suggests that the number of defects in these GaInP nanowires is smaller, compared to nanowires with similar composition but grown with the TMGa precursor.

In conclusion, the findings of Paper III support the use of the Ga precursor TEGa for the growth of GaInP nanowire segments.

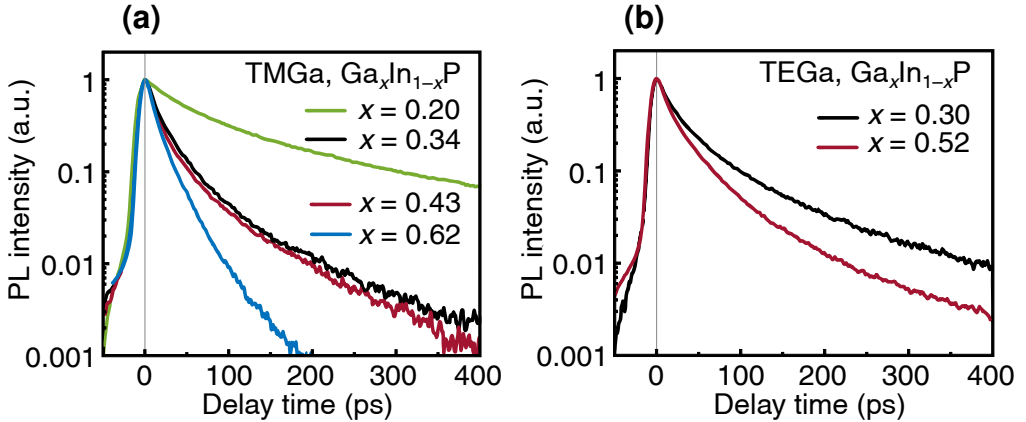


**Figure 5.6:** Composition-dependent TRPL decays of GaInP nanowire arrays. The GaInP nanowire composition is indicated in the legend. (a) Nanowires grown using TMGa (b) Nanowires grown using TEGa. Figures adapted from Paper III.

### 5.3 Processing and Characterization of GaInP/InP Tandem Junction Nanowire Solar Cells – Results of Paper IV

The topic of Paper IV are tandem junction GaInP/InP nanowire solar cells. In previous work in our group, nanowires containing a GaInP/InP double junction as well as nanowires containing a GaInP/InP/InAsP triple junction were realized and characterized in single-nanowire form [110, 111]. Devices based on arrays of tandem junction nanowires, connecting thousands of nanowires in parallel, have not been manufactured previously.

In Paper IV, tandem junction GaInP/InP nanowire solar cells with different compositions of the top junction GaInP material are presented. As the GaInP composition is changed, the band gap of the top junction is shifted, changing the parts of the solar spectrum absorbed in either subcell. The expectation is that a higher Ga content will lead to a larger band gap of the GaInP material and thus an onset of absorption at a shorter wavelength. The EQE measurements presented in Paper IV, reprinted in Figure 5.7, follow this expectation. As the absorption range of the GaInP top cell changes, the EQE of the InP bottom cell is also affected. Only the light passing through the GaInP cell, which is mostly the light with an energy below the GaInP band gap, is available to the InP subcell. This means that the EQE plot can be roughly divided into two regions,

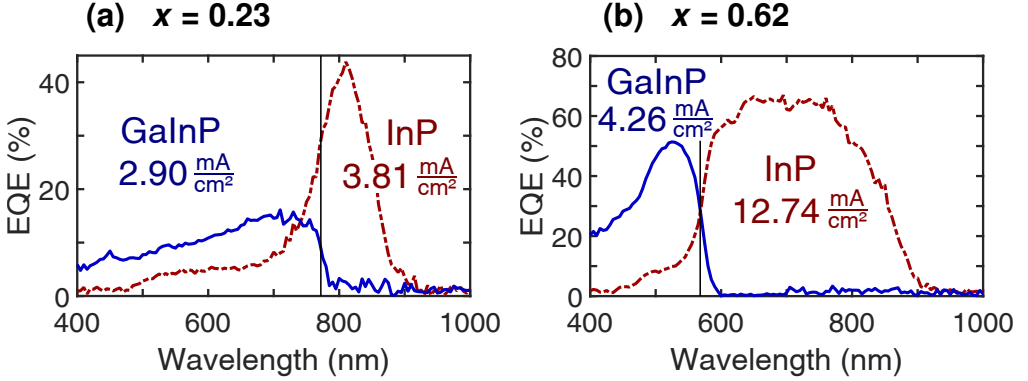


**Figure 5.7:** EQE of the GaInP and InP sub-cells of GaInP/InP tandem junction nanowire solar cells. The top cell  $\text{Ga}_x\text{In}_{1-x}\text{P}$  composition differs between the samples, and the Ga content  $x$  is indicated in the caption of each panel. The short-circuit current density  $J_{\text{SC}}$  as calculated from the product of the sub-cell EQE with the solar spectrum is given. Figures adapted from Paper IV.

with most absorption happening in the GaInP (InP) subcell for energies above (below) the GaInP band gap, respectively.

For each EQE curve of a subcell, the current density expected from that subcell is indicated, calculated as the integral of the EQE multiplied by the spectral irradiance of the solar illumination,

$$J_{\text{SC}} = \int \text{EQE}(\lambda) \cdot F_{\text{AM1.5G}}(\lambda) d\lambda$$

Due to the low EQE of the GaInP subcell,  $J_{\text{SC}}^{\text{GaInP}} < J_{\text{SC}}^{\text{InP}}$  for all of the solar cells, which means that the GaInP subcell is current limiting.

Figure 5.8 shows  $J$ - $V$  measurements performed on the same devices. As expected from the EQE of the current limiting GaInP subcell, the  $J_{\text{SC}}$  of the GaInP/InP tandem junction solar cells is quite low, and is in approximate agreement with the values calculated from the GaInP subcell EQE.

As described in section 5.1.2, the voltages of the subcells add to the total voltage of the tandem junction device. This means that we can expect an open circuit voltage  $V_{\text{OC}}$  larger than the  $V_{\text{OC}}$  of either subcell. This is confirmed by the  $J$ - $V$  measurements shown in Figure 5.8, with the  $V_{\text{OC}}$  of different devices ranging between 1.37 – 1.91 V, depending on the GaInP composition. With increasing Ga content of the GaInP, the total  $V_{\text{OC}}$  of the GaInP/InP tandem junction solar cells increases. This is in agreement with the increase of the GaInP band gap and thus GaInP subcell  $V_{\text{OC}}$ .

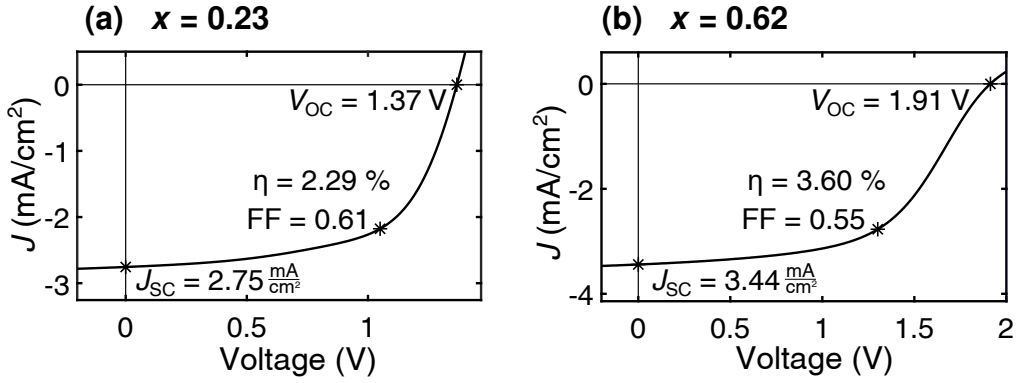


**Figure 5.8:**  $J$ – $V$  curves of GaInP/InP tandem junction nanowire solar cells under AM1.5G illumination. The top cell  $\text{Ga}_x\text{In}_{1-x}\text{P}$  composition differs between the samples, and the Ga content  $x$  is indicated in the caption of each panel. Values of  $J_{SC}$ ,  $V_{OC}$ , FF and solar conversion efficiency  $\eta$  are given. Figures adapted from Paper IV.

In conclusion, Paper IV reports on the manufacturing of nanowire tandem junction solar cells using the GaInP/InP materials system. Further improvement of the solar cells is needed to achieve a competitive efficiency, most importantly by optimizing the GaInP subcell.



## 6 Outlook

The work presented in this thesis attempts to inspire and inform further progress in the development of III–V nanowire solar cells. Paper I has demonstrated the feasibility of relatively large area InP nanowire solar cell fabrication, which could enable commercial viability in niche applications, such as solar cells for spacecraft. Current limitations were also shown, inspiring further work to improve the front contacting scheme.

The use of the TEGa precursor in Paper III to grow GaInP segments resulting in high quality according to the observed TRPL lifetimes has informed the use of TEGa as a Ga precursor in the development of the GaInP/InP tandem junction nanowires. The successful fabrication of tandem junction nanowire solar cells in Paper IV presents a milestone of nanowire solar cell development. The successful open circuit voltage addition demonstrates the proper functioning of the GaInP and InP subcells connected by the Esaki tunnel diode. However, due to the low quantum efficiency of the current-limiting GaInP subcell, the tandem junction device is far from exceeding the single junction Shockley–Queisser limit. Further work thus has to focus on improving the GaInP subcell. As surface defects are assumed to be responsible for the low performance of the GaInP subcell, surface passivation of the GaInP nanowire segment needs to be explored. The necessity to find a surface passivation scheme that works well for both subcells of the tandem junction nanowire could present a further challenge in these efforts.

After achieving a GaInP subcell with a good quantum efficiency, current matching between the GaInP and InP subcells will become relevant for achieving a high overall efficiency. As a next step, a third subcell, for example the low band gap InAsP could be introduced, further increasing the theoretical efficiency limit, but also risking to introduce challenges concerning passivation, current matching and processing.

In terms of cost reduction, the synthesis of nanowires at a large scale is paramount. The results presented in Paper I concerning growth and processing on 2-inch wafers are a first step in this direction, but much more work is needed to make the III–V nanowire solar cells cost-competitive. Of course, this will have to include a strategy to re-use the expensive III–V substrates, for example based on the concept of nanowire array peel-off used in Paper II. However, the cost reductions with such an approach are limited, comparable to the case of epitaxial lift-off for planar III–V devices [60]. Direct competition with established Si solar cells is thus not realistic in the foreseeable future, and the possible applications of nanowire solar cells are cost-insensitive niche markets such as solar cells for spacecraft, and possibly building-integrated photovoltaics. Assuming that the current challenges can be overcome, highly efficient III–V nanowire solar cells might present themselves as an attractive option for these applications.

# References

- [1] Fernando Racimo, Elia Valentini, Gaston Rijo De León, Teresa L. Santos, Anna Norberg, Lane M. Atmore, Myranda Murray, Sanja M. Hakala, Frederik Appel Olsen, Charlie J. Gardner, and Julia B. Halder. The biospheric emergency calls for scientists to change tactics. *eLife*, 11:e83292, 2022.
- [2] Timothy M. Lenton, Chi Xu, Jesse F. Abrams, Ashish Ghadiali, Sina Loriani, Boris Sakshewski, Caroline Zimm, Kristie L. Ebi, Robert R. Dunn, Jens-Christian Svenning, and Marten Scheffer. Quantifying the human cost of global warming. *Nature Sustainability*, 6(10):1237–1247, 2023.
- [3] Luke Kemp, Chi Xu, Joanna Depledge, Kristie L. Ebi, Goodwin Gibbins, Timothy A. Kohler, Johan Rockström, Marten Scheffer, Hans Joachim Schellnhuber, Will Steffen, and Timothy M. Lenton. Climate endgame: Exploring catastrophic climate change scenarios. *Proceedings of the National Academy of Sciences*, 119(34):e2108146119, 2022.
- [4] Gerardo Ceballos, Paul R. Ehrlich, and Rodolfo Dirzo. Biological annihilation via the ongoing sixth mass extinction signaled by vertebrate population losses and declines. *Proceedings of the National Academy of Sciences*, 114(30), 2017.
- [5] Pieter Trans (NOAA) and Ralph Keeling (Scripps Institution of Oceanography). Trends in atmospheric carbon dioxide. NOAA Global Monitoring Laboratory. URL <https://gml.noaa.gov/ccgg/trends/data.html>.
- [6] Hans Hersbach, Bill Bell, Paul Berrisford, Shoji Hirahara, András Horányi, Joaquín Muñoz-Sabater, Julien Nicolas, Carole Peubey, Raluca Radu, Dinand Schepers, Adrian Simmons, Cornel Soci, Saleh Abdalla, Xavier Abellan, Gianpaolo Balsamo, Peter Bechtold, Gionata Biavati, Jean Bidlot, Massimo Bonavita, Giovanna De Chiara, Per Dahlgren, Dick Dee, Michail Diamantakis, Rossana Dragani, Johannes Flemming, Richard Forbes, Manuel Fuentes, Alan Geer, Leo Haimberger, Sean Healy, Robin J. Hogan, Elías Hólm, Marta Janisková, Sarah Keeley, Patrick Laloyaux, Philippe Lopez, Cristina Lupu, Gabor Radnoti, Patricia De Rosnay, Iryna Rozum, Freja Vamborg, Sébastien Villaume, and Jean-Noël Thépaut. The ERA5 global reanalysis. *Quarterly Journal of the Royal Meteorological Society*, 146(730):1999–2049, 2020.
- [7] Copernicus Climate Change Service. 2023 is the hottest year on record, with global temperatures close to the 1.5°C limit. URL <https://climate.copernicus.eu/copernicus-2023-hottest-year-record>.

- [8] David I. Armstrong McKay, Arie Staal, Jesse F. Abrams, Ricarda Winkelmann, Boris Sakschewski, Sina Loriani, Ingo Fetzer, Sarah E. Cornell, Johan Rockström, and Timothy M. Lenton. Exceeding 1.5°C global warming could trigger multiple climate tipping points. *Science*, 377(6611):eabn7950, 2022.
- [9] Robin D. Lamboll, Zebedee R. J. Nicholls, Christopher J. Smith, Jarmo S. Kikstra, Edward Byers, and Joeri Rogelj. Assessing the size and uncertainty of remaining carbon budgets. *Nature Climate Change*, 13:1360–1367, 2023.
- [10] Isak Stoddard, Kevin Anderson, Stuart Capstick, Wim Carton, Joanna Depledge, Keri Facer, Clair Gough, Frederic Hache, Claire Hoolohan, Martin Hultman, Niclas Hällström, Sivan Kartha, Sonja Klinsky, Magdalena Kuchler, Eva Lövbrand, Naghmeh Nasiritousi, Peter Newell, Glen P. Peters, Youba Sokona, Andy Stirling, Matthew Stilwell, Clive L. Spash, and Mariama Williams. Three decades of climate mitigation: Why haven’t we bent the global emissions curve? *Annual Review of Environment and Resources*, 46(1): 653–689, 2021.
- [11] Kate Raworth. *Doughnut Economics: Seven Ways to Think Like a 21st-Century Economist*. Chelsea Green Publishing, 2017. ISBN 978-16-035-8674-0.
- [12] IPCC. Climate change 2023: Synthesis report. Contribution of working groups I, II and III to the Sixth Assessment Report of the Intergovernmental Panel on Climate Change [Core writing team, H. Lee and J. Romero (eds.)], 2023.
- [13] International Energy Agency (IEA). Renewables 2023.
- [14] International Energy Agency (IEA). Renewables 2020 – analysis and forecast to 2025.
- [15] International Renewable Energy Agency – processed by Our World in Data. Solar energy capacity, dataset from renewable electricity capacity and generation statistics, 2023. URL <https://ourworldindata.org/grapher/installed-solar-pv-capacity>.
- [16] Galen Barbose, Naïm Darghouth, Eric O’Shaughnessy, and Sydney Forrester. Lawrence Berkeley National Laboratory. Tracking the sun – pricing and design trends for distributed photovoltaic systems in the United States, 2023.
- [17] S. Ranjan, S. Balaji, Rocco A. Panella, and B. Erik Ydstie. Silicon solar cell production. *Computers & Chemical Engineering*, 35(8):1439–1453, 2011.
- [18] Martin A. Green. Commercial progress and challenges for photovoltaics. *Nature Energy*, 1(1):15015, 2016.
- [19] John F. Geisz, Ryan M. France, Kevin L. Schulte, Myles A. Steiner, Andrew G. Norman, Harvey L. Guthrey, Matthew R. Young, Tao Song, and Thomas Moriarty. Six-junction III–V solar cells with 47.1% conversion efficiency under 143 Suns concentration. *Nature Energy*, 5(4):326–335, 2020.
- [20] Nicklas Anttu and Hongqi Xu. Efficient light management in vertical nanowire arrays for photovoltaics. *Optics Express*, 21(S3):A558, 2013.
- [21] Ningfeng Huang, Chenxi Lin, and Michelle L. Povinelli. Broadband absorption of semiconductor nanowire arrays for photovoltaic applications. *Journal of Optics*, 14(2):024004, 2012.

- [22] Lukas Hrachowina, Yuwei Zhang, Aditya Saxena, Gerald Siefer, Enrique Barrigon, and Magnus T. Borgström. Development and characterization of a bottom-up InP nanowire solar cell with 16.7% efficiency. In *2020 47th IEEE Photovoltaic Specialists Conference (PVSC)*, pages 1754–1756, 2020.
- [23] Dick van Dam, Niels J. J. van Hoof, Yingchao Cui, Peter J. van Veldhoven, Erik P. A. M. Bakkers, Jaime Gómez Rivas, and Jos E. M. Haverkort. High-efficiency nanowire solar cells with omnidirectionally enhanced absorption due to self-aligned indium-tin-oxide Mie scatterers. *ACS Nano*, 10(12):11414–11419, 2016.
- [24] Vidur Raj, Kaushal Vora, Lan Fu, H. Hoe Tan, and Chennupati Jagadish. High-efficiency solar cells from extremely low minority carrier lifetime substrates using radial junction nanowire architecture. *ACS Nano*, 13(10):12015–12023, 2019.
- [25] Magnus T. Borgström, Martin H. Magnusson, Frank Dimroth, Gerald Siefer, Oliver Höhn, Heike Riel, Heinz Schmid, Stephan Wirths, Mikael Björk, Ingvar Åberg, Willie Peijnenburg, Martina Vijver, Maria Tchernycheva, Valerio Piazza, and Lars Samuelson. Towards nanowire tandem junction solar cells on silicon. *IEEE Journal of Photovoltaics*, 8(3):733–740, 2018.
- [26] Larry Partain and Lewis Fraas. *Solar Cells and their Applications*. John Wiley & Sons, 2010. ISBN 978-0-470-44633-1.
- [27] D. M. Chapin, C. S. Fuller, and G. L. Pearson. A new silicon p–n junction photocell for converting solar radiation into electrical power. *Journal of Applied Physics*, 25(5): 676–677, 1954.
- [28] Charles Kittel. *Introduction to Solid State Physics*. John Wiley & Sons, Inc, 8th edition, 2005. ISBN 0-471-41526-X.
- [29] Albert Polman and Harry A. Atwater. Photonic design principles for ultrahigh-efficiency photovoltaics. *Nature Materials*, 11(3):174–177, 2012.
- [30] J. William Shockley. Detailed balance limit of efficiency of p–n junction solar cells. *Journal of Applied Physics*, 32(3):510–519, 1961.
- [31] Sven Rühle. Tabulated values of the Shockley–Queisser limit for single junction solar cells. *Solar Energy*, 130:139–147, 2016.
- [32] Marius Grundmann. *The Physics of Semiconductors: An Introduction Including Nanophysics and Applications*. Springer International Publishing, 2016. ISBN 978-3-319-23879-1.
- [33] Fraunhofer Institute for Solar Energy Systems. Photovoltaics report, 2022.
- [34] Arnaud de La Tour, Matthieu Glachant, and Yann Ménière. What cost for photovoltaic modules in 2020? Lessons from experience curve models. *hal-00805668*, 2013.
- [35] Radovan Kopecek, Florian Buchholz, Valentin D. Mihailetschi, Joris Libal, Jan Lossen, Ning Chen, Haifeng Chu, Christoph Peter, Tudor Timofte, Andreas Halm, Yonggang Guo, Xiaoyong Qu, Xiang Wu, Jiaqing Gao, and Peng Dong. Interdigitated back contact technology as final evolution for industrial crystalline single-junction silicon solar cell. *Solar*, 3(1):1–14, 2022.

- [36] Lucio Claudio Andreani, Angelo Bozzola, Piotr Kowalczewski, Marco Liscidini, and Lisa Redorici. Silicon solar cells: Toward the efficiency limits. *Advances in Physics: X*, 4(1):1548305, 2019.
- [37] Kunta Yoshikawa, Hayato Kawasaki, Wataru Yoshida, Toru Irie, Katsunori Konishi, Kunihiko Nakano, Toshihiko Uto, Daisuke Adachi, Masanori Kanematsu, Hisashi Uzu, and Kenji Yamamoto. Silicon heterojunction solar cell with interdigitated back contacts for a photoconversion efficiency over 26%. *Nature Energy*, 2(5):17032, 2017.
- [38] Martin A. Green, Yoshihiro Hishikawa, Wilhelm Warta, Ewan D. Dunlop, Dean H. Levi, Jochen Hohl-Ebinger, and Anita W. H. Ho-Baillie. Solar cell efficiency tables (version 50). *Progress in Photovoltaics: Research and Applications*, 25(7):668–676, 2017.
- [39] Bruno Ehrler, Esther Alarcón-Lladó, Stefan W. Tabernig, Tom Veeken, Erik C. Garnett, and Albert Polman. Photovoltaics reaching for the Shockley–Queisser limit. *ACS Energy Letters*, 5(9):3029–3033, 2020.
- [40] John C. C. Fan. Basic concepts for the design of high-efficiency single-junction and multibandgap solar cells. In *Proc. SPIE 0543, Photovoltaics*, 1985.
- [41] Zhe Liu, Sarah E. Sofia, Hannu S. Laine, Michael Woodhouse, Sarah Wieghold, Ian Marius Peters, and Tonio Buonassisi. Revisiting thin silicon for photovoltaics: a technoeconomic perspective. *Energy & Environmental Science*, 13(1):12–23, 2020.
- [42] Giancarlo C. Righini and Francesco Enrichi. Solar cells’ evolution and perspectives: a short review. In *Solar Cells and Light Management*, pages 1–32. Elsevier, 2020. ISBN 978-0-08-102762-2.
- [43] K. L. Chopra, P. D. Paulson, and V. Dutta. Thin-film solar cells: an overview. *Progress in Photovoltaics: Research and Applications*, 12(2-3):69–92, 2004.
- [44] Martin A. Green. Thin-film solar cells: review of materials, technologies and commercial status. *Journal of Materials Science: Materials in Electronics*, 18(S1):15–19, 2007.
- [45] Moritz Riede, Donato Spoltore, and Karl Leo. Organic solar cells – the path to commercial success. *Advanced Energy Materials*, 11(1):2002653, 2021.
- [46] Hailin Zhang, Xu Ji, Haoyi Yao, Quanhai Fan, Bowen Yu, and Jishu Li. Review on efficiency improvement effort of perovskite solar cell. *Solar Energy*, 233:421–434, 2022.
- [47] Pengyu Zhang, Menglin Li, and Wen-Cheng Chen. A perspective on perovskite solar cells: Emergence, progress, and commercialization. *Frontiers in Chemistry*, 10:802890, 2022.
- [48] Nam-Gyu Park. Perovskite solar cells: an emerging photovoltaic technology. *Materials Today*, 18(2):65–72, 2015.
- [49] Ritika Sharma, Arushi Sharma, Shikha Agarwal, and M. S. Dhaka. Stability and efficiency issues, solutions and advancements in perovskite solar cells: A review. *Solar Energy*, 244:516–535, 2022.

- [50] Randi Azmi, Esma Ugur, Akmaral Seitkhan, Faisal Aljamaan, Anand S. Subbiah, Jiang Liu, George T. Harrison, Mohamad I. Nugraha, Mathan K. Eswaran, Maxime Babics, Yuan Chen, Fuzong Xu, Thomas G. Allen, Atteq Ur Rehman, Chien-Lung Wang, Thomas D. Anthopoulos, Udo Schwingenschlögl, Michele De Bastiani, Erkan Aydin, and Stefaan De Wolf. Damp heat-stable perovskite solar cells with tailored-dimensionality 2D/3D heterojunctions. *Science*, 376(6588):73–77, 2022.
- [51] Masafumi Yamaguchi, Akio Yamamoto, Naoto Uchida, and Chikao Uemura. A new approach for thin film InP solar cells. *Solar Cells*, 19(1):85–96, 1986.
- [52] National Renewable Energy Laboratory. NREL best research-cell efficiency chart, 2023. URL <https://www.nrel.gov/pv/assets/pdfs/best-research-cell-efficiencies.pdf>.
- [53] E. A. Alsema, R. F. A. Cuelenaere, and W. C. Turkenburg. Cost perspectives of GaAs thin-film solar cells. In *Tenth E.C. Photovoltaic Solar Energy Conference*, pages 563–566, 1991.
- [54] Edward M. Gaddy. Cost trade between multijunction, gallium arsenide and silicon solar cells. *Progress in Photovoltaics: Research and Applications*, 4(2):155–161, 1996.
- [55] P. Pérez-Higueras, E. Muñoz, G. Almonacid, and P.G. Vidal. High concentrator photovoltaics efficiencies: Present status and forecast. *Renewable and Sustainable Energy Reviews*, 15(4):1810–1815, 2011.
- [56] P. A. Iles. Evolution of space solar cells. *Solar Energy Materials & Solar Cells*, 68:1–13, 2001.
- [57] H. L. Cotal, D. R. Lillington, J. H. Ermer, R. R. King, N. H. Karam, S. R. Kurtz, D. J. Friedman, J. M. Olson, S. Ward, A. Duda, K. A. Emery, and T. Moriarty. Highly efficient 32.3% monolithic GaInP/GaAs/Ge triple junction concentrator solar cells. *NCPV Proceedings*, pages 111–112, 2000.
- [58] Kelsey A. Horowitz, Timothy W. Remo, Brittany Smith, and Aaron Ptak. National Renewable Energy Laboratory (NREL). A techno-economic analysis and cost reduction roadmap for III–V solar cells, 2018.
- [59] Ryan M. France, Frank Dimroth, Tyler J. Grassman, and Richard R. King. Metamorphic epitaxy for multijunction solar cells. *MRS Bulletin*, 41(3):202–209, 2016.
- [60] J. Scott Ward, Timothy Remo, Kelsey Horowitz, Michael Woodhouse, Bhushan Sopori, Kaitlyn VanSant, and Paul Basore. Techno-economic analysis of three different substrate removal and reuse strategies for III–V solar cells. *Progress in Photovoltaics: Research and Applications*, 24(9):1284–1292, 2016.
- [61] Peidong Yang, Ruoxue Yan, and Melissa Fardy. Semiconductor nanowire: What’s next? *Nano Letters*, 10(5):1529–1536, 2010.
- [62] Magnus W. Larsson, Jakob B. Wagner, Mathias Wallin, Paul Håkansson, Linus E. Fröberg, Lars Samuelson, and L. Reine Wallenberg. Strain mapping in free-standing heterostructured wurtzite InAs/InP nanowires. *Nanotechnology*, 18(1):015504, 2007.

- [63] María de la Mata, César Magén, Philippe Caroff, and Jordi Arbiol. Atomic scale strain relaxation in axial semiconductor III–V nanowire heterostructures. *Nano Letters*, 14(11):6614–6620, 2014.
- [64] Thomas Mårtensson, Patrik T. Svensson, Brent A. Wacaser, Magnus W. Larsson, Werner Seifert, Knut Deppert, Anders Gustafsson, L. Reine Wallenberg, and Lars Samuelson. Epitaxial III–V nanowires on silicon. *Nano Letters*, 4(10):1987–1990, 2004.
- [65] Ruoxue Yan, Daniel Gargas, and Peidong Yang. Nanowire photonics. *Nature Photonics*, 3(10):569–576, 2009.
- [66] Di Liang and John E. Bowers. Recent progress in heterogeneous III–V-on-silicon photonic integration. *Light: Advanced Manufacturing*, 2:5, 2021.
- [67] Joan M. Ramirez, Stephane Malhouitre, Kamil Gradkowski, Padraic E. Morrissey, Peter O’Brien, Christophe Caillaud, Nicolas Vaissiere, Jean Decobert, Shenghui Lei, Ryan Enright, Alexandre Shen, Hajar Elfaiki, Mohand Achouche, Theo Verolet, Claire Besancon, Antonin Gallet, Delphine Neel, Karim Hassan, Segolene Olivier, and Christophe Jany. III–V-on-silicon integration: From hybrid devices to heterogeneous photonic integrated circuits. *IEEE Journal of Selected Topics in Quantum Electronics*, 26(2):6100213, 2020.
- [68] Alan Y. Liu and John Bowers. Photonic integration with epitaxial III–V on silicon. *IEEE Journal of Selected Topics in Quantum Electronics*, 24(6):6000412, 2018.
- [69] Mattias Borg, Heinz Schmid, Kirsten E. Moselund, Giorgio Signorello, Lynne Gignac, John Bruley, Chris Breslin, Pratyush Das Kanungo, Peter Werner, and Heike Riel. Vertical III–V nanowire device integration on Si(100). *Nano Letters*, 14(4):1914–1920, 2014.
- [70] Heike Riel, Lars-Erik Wernersson, Minghwei Hong, and Jesús A. Del Alamo. III–V compound semiconductor transistors – from planar to nanowire structures. *MRS Bulletin*, 39(8):668–677, 2014.
- [71] Katsuhiko Tomioka, Tomotaka Tanaka, Shinjiro Hara, Kenji Hiruma, and Takashi Fukui. III–V nanowires on Si substrate: Selective-area growth and device applications. *IEEE Journal of Selected Topics in Quantum Electronics*, 17(4):1112–1129, 2011.
- [72] Svenja Mauthe, Yannick Baumgartner, Marilyne Sousa, Qian Ding, Marta D. Rossell, Andreas Schenk, Lukas Czornomaz, and Kirsten E. Moselund. High-speed III–V nanowire photodetector monolithically integrated on Si. *Nature Communications*, 11(1):4565, 2020.
- [73] Hyunseok Kim, Wook-Jae Lee, Alan C. Farrell, Juan S. D. Morales, Pradeep Senanayake, Sergey V. Prikhodko, Tomasz J. Ochalski, and Diana L. Huffaker. Monolithic InGaAs nanowire array lasers on silicon-on-insulator operating at room temperature. *Nano Letters*, 17(6):3465–3470, 2017.
- [74] Gregor Koblmüller, Benedikt Mayer, Thomas Stettner, Gerhard Abstreiter, and Jonathan J. Finley. GaAs–AlGaAs core–shell nanowire lasers on silicon: invited review. *Semiconductor Science and Technology*, 32(5):053001, 2017.
- [75] Enrique Barrigón, Magnus Heurlin, Zhaoxia Bi, Bo Monemar, and Lars Samuelson. Synthesis and applications of III–V nanowires. *Chemical Reviews*, 119(15):9170–9220, 2019.

- [76] Sebastian Lehmann, Daniel Jacobsson, and Kimberly A. Dick. Crystal phase control in GaAs nanowires: opposing trends in the Ga- and As-limited growth regimes. *Nanotechnology*, 26(30):301001, 2015.
- [77] Sebastian Lehmann, Jesper Wallentin, Daniel Jacobsson, Knut Deppert, and Kimberly A. Dick. A general approach for sharp crystal phase switching in InAs, GaAs, InP, and GaP nanowires using only group V flow. *Nano Letters*, 13(9):4099–4105, 2013.
- [78] Rudolph S. Wagner and W. Chadwick Ellis. Vapor–liquid–solid mechanism of single crystal growth. *Applied Physics Letters*, 4(5):89–90, 1964.
- [79] M. Yazawa, M. Koguchi, A. Muto, M. Ozawa, and K. Hiruma. Effect of one monolayer of surface gold atoms on the epitaxial growth of InAs nanowhiskers. *Applied Physics Letters*, 61(17):2051–2053, 1992.
- [80] Keiichi Haraguchi, Toshio Katsuyama, Kenji Hiruma, and Kensuke Ogawa. GaAs p–n junction formed in quantum wire crystals. *Applied Physics Letters*, 60(6):745–747, 1992.
- [81] Kenji Hiruma, Hisaya Murakoshi, Masamitsu Yazawa, and Toshio Katsuyama. Self-organized growth of GaAs/InAs heterostructure nanocylinders by organometallic vapor phase epitaxy. *Journal of Crystal Growth*, 163:226–231, 1996.
- [82] Nicklas Anttu, Alireza Abrand, Damir Asoli, Magnus Heurlin, Ingvar Åberg, Lars Samuelson, and Magnus T. Borgström. Absorption of light in InP nanowire arrays. *Nano Research*, 7(6):816–823, 2014.
- [83] Jesper Wallentin, Nicklas Anttu, Damir Asoli, Maria Huffman, Ingvar Åberg, Martin H. Magnusson, Gerald Siefer, Peter Fuss-Kailuweit, Frank Dimroth, Bernd Witzigmann, H. Q. Xu, Lars Samuelson, Knut Deppert, and Magnus T. Borgström. InP nanowire array solar cells achieving 13.8% efficiency by exceeding the ray optics limit. *Science*, 339(6123):1057–1060, 2013.
- [84] Silke L. Diedenhofen, Olaf T. A. Janssen, Grzegorz Grzela, Erik P. A. M. Bakkers, and Jaime Gómez Rivas. Strong geometrical dependence of the absorption of light in arrays of semiconductor nanowires. *ACS Nano*, 5(3):2316–2323, 2011.
- [85] Yunlu Xu, Tao Gong, and Jeremy N. Munday. The generalized Shockley–Queisser limit for nanostructured solar cells. *Scientific Reports*, 5(1):13536, 2015.
- [86] Nicklas Anttu. Shockley–Queisser detailed balance efficiency limit for nanowire solar cells. *ACS Photonics*, 2(3):446–453, 2015.
- [87] Pilar Espinet-Gonzalez, Enrique Barrigón, Yang Chen, Gaute Otnes, Giuliano Vescovi, Colin Mann, John V. Lloyd, Don Walker, Michael D. Kelzenberg, Ingvar Åberg, Magnus T. Borgström, Lars Samuelson, and Harry A. Atwater. Nanowire solar cells: A new radiation hard PV technology for space applications. *IEEE Journal of Photovoltaics*, 10(2):502–507, 2020.
- [88] Pilar Espinet-Gonzalez, Enrique Barrigón, Gaute Otnes, Giuliano Vescovi, Colin Mann, Ryan M. France, Alex J. Welch, Matthew S. Hunt, Don Walker, Michael D. Kelzenberg, Ingvar Åberg, Magnus T. Borgström, Lars Samuelson, and Harry A. Atwater. Radiation tolerant nanowire array solar cells. *ACS Nano*, 13(11):12860–12869, 2019.

- [89] Gaute Otnes and Magnus T. Borgström. Towards high efficiency nanowire solar cells. *Nano Today*, 12:31–45, 2017.
- [90] Vidur Raj, Tuomas Haggren, Wei W. Wong, Hark H. Tan, and Chennupati Jagadish. Topical review: pathways toward cost-effective single-junction III–V solar cells. *Journal of Physics D: Applied Physics*, 55(14):143002, 2022.
- [91] Joshua M. Spurgeon, Katherine E. Plass, Brendan M. Kayes, Bruce S. Brunschwig, Harry A. Atwater, and Nathan S. Lewis. Repeated epitaxial growth and transfer of arrays of patterned, vertically aligned, crystalline Si wires from a single Si(111) substrate. *Applied Physics Letters*, 93(3):032112, 2008.
- [92] A. J. Standing, S. Assali, Jos E. M. Haverkort, and Erik P. A. M. Bakkers. High yield transfer of ordered nanowire arrays into transparent flexible polymer films. *Nanotechnology*, 23(49):495305, 2012.
- [93] Alessandro Cavalli, Alain Dijkstra, Jos E. M. Haverkort, and Erik P. A. M. Bakkers. Nanowire polymer transfer for enhanced solar cell performance and lower cost. *Nano-Structures & Nano-Objects*, 16:59–62, 2018.
- [94] Xing Dai, Agnes Messanvi, Hezhi Zhang, Christophe Durand, Joël Eymery, Catherine Bougerol, François H. Julien, and Maria Tchernycheva. Flexible light-emitting diodes based on vertical nitride nanowires. *Nano Letters*, 15(10):6958–6964, 2015.
- [95] Muyi Chen, Eiji Nakai, Katsuhiko Tomioka, and Takashi Fukui. Application of free-standing InP nanowire arrays and their optical properties for resource-saving solar cells. *Applied Physics Express*, 8(1):012301, 2015.
- [96] Reza Jafari Jam, Jason P. Beech, Xulu Zeng, Jonas Johansson, Lars Samuelson, Håkan Pettersson, and Magnus T. Borgström. Embedded sacrificial AlAs segments in GaAs nanowires for substrate reuse. *Nanotechnology*, 31(20):204002, 2020.
- [97] Yuwei Zhang, Lukas Hrachowina, Enrique Barrigon, Ingvar Åberg, and Magnus T. Borgström. Self-limiting polymer exposure for vertical processing of semiconductor nanowire-based flexible electronics. *ACS Applied Nano Materials*, 3(8):7743–7749, 2020.
- [98] Yang Chen, Lukas Hrachowina, Enrique Barrigon, Jason P. Beech, David Alcer, Roman Lyttleton, Reza Jafari Jam, Lars Samuelson, Heiner Linke, and Magnus T. Borgström. Semiconductor nanowire array for transparent photovoltaic applications. *Applied Physics Letters*, 118(19):191107, 2021.
- [99] Magnus Heurlin, Martin H. Magnusson, David Lindgren, Martin Ek, L. Reine Wallenberg, Knut Deppert, and Lars Samuelson. Continuous gas-phase synthesis of nanowires with tunable properties. *Nature*, 492(7427):90–94, 2012.
- [100] Fangfang Yang, Maria E. Messing, Kilian Mergenthaler, Masoomah Ghasemi, Jonas Johansson, L. Reine Wallenberg, Mats-Erik Pistol, Knut Deppert, Lars Samuelson, and Martin H. Magnusson. Zn-doping of GaAs nanowires grown by aerotaxy. *Journal of Crystal Growth*, 414:181–186, 2015.
- [101] Wondwosen Metaferia, Axel R. Persson, Kilian Mergenthaler, Fangfang Yang, Wei Zhang, Arkady Yartsev, Reine Wallenberg, Mats-Erik Pistol, Knut Deppert, Lars Samuelson, and Martin H. Magnusson. GaAsP nanowires grown by aerotaxy. *Nano Letters*, 16(9):5701–5707, 2016.

- [102] Enrique Barrigón, Olof Hultin, David Lindgren, Farnaz Yadegari, Martin H. Magnusson, Lars Samuelson, L. I. M. Johansson, and Mikael T. Björk. GaAs nanowire p–n junctions produced by low cost and high-throughput aerotaxy. *Nano Letters*, 18(2):1088–1092, 2018.
- [103] Vidur Raj, Hark H. Tan, and Chennupati Jagadish. Axial vs. radial junction nanowire solar cell. *arXiv preprint*, arXiv:2103.13190, 2021.
- [104] Ingvar Åberg, Giuliano Vescovi, Damir Asoli, Umeair Naseem, James P. Gilboy, Christian Sundvall, Andreas Dahlgren, K. Erik Svensson, Nicklas Anttu, Mikael T. Björk, and Lars Samuelson. A GaAs nanowire array solar cell with 15.3% efficiency at 1 sun. *IEEE Journal of Photovoltaics*, 6(1):185–190, 2016.
- [105] Maoqing Yao, Ningfeng Huang, Sen Cong, Chun-Yung Chi, M. Ashkan Seyedi, Yen-Ting Lin, Yu Cao, Michelle L. Povinelli, P. Daniel Dapkus, and Chongwu Zhou. GaAs nanowire array solar cells with axial p–i–n junctions. *Nano Letters*, 14(6):3293–3303, 2014.
- [106] Qian Gao, Ziyuan Li, Li Li, Kaushal Vora, Zhe Li, Ahmed Alabadla, Fan Wang, Yanan Guo, Kun Peng, Yesaya C. Wenas, Sudha Mokkaapati, Fouad Karouta, Hark Hoe Tan, Chennupati Jagadish, and Lan Fu. Axial p–n junction design and characterization for InP nanowire array solar cells. *Progress in Photovoltaics: Research and Applications*, 27(3):237–244, 2019.
- [107] Parsian K. Mohseni, Ashkan Behnam, Joshua D. Wood, Xiang Zhao, Ki Jun Yu, Ning C. Wang, Angus Rockett, John A. Rogers, Joseph W. Lyding, Eric Pop, and Xiuling Li. Monolithic III-V nanowire solar cells on graphene via direct van der Waals epitaxy. *Advanced Materials*, 26(22):3755–3760, 2014.
- [108] Jonathan P. Boulanger, A. C. E. Chia, Brendan A. Wood, S. Yazdi, T. Kasama, Martin Aagesen, and Ray R. LaPierre. Characterization of a Ga-assisted GaAs nanowire array solar cell on Si substrate. *IEEE Journal of Photovoltaics*, 6(3):661–667, 2016.
- [109] Maoqing Yao, Sen Cong, Shermin Arab, Ningfeng Huang, Michelle L. Povinelli, Stephen B. Cronin, P. Daniel Dapkus, and Chongwu Zhou. Tandem solar cells using GaAs nanowires on Si: Design, fabrication, and observation of voltage addition. *Nano Letters*, 15(11):7217–7224, 2015.
- [110] Lukas Hrachowina, Enrique Barrigón, and Magnus T. Borgström. Development and characterization of photovoltaic tandem-junction nanowires using electron-beam-induced current measurements. *Nano Research*, 15(9):8510–8515, 2022.
- [111] Lukas Hrachowina, Yang Chen, Enrique Barrigón, Reine Wallenberg, and Magnus T. Borgström. Realization of axially defined GaInP/InP/InAsP triple-junction photovoltaic nanowires for high-performance solar cells. *Materials Today Energy*, 27:101050, 2022.
- [112] Helmut Schift. Nanoimprint lithography: An old story in modern times? A review. *Journal of Vacuum Science & Technology B: Microelectronics and Nanometer Structures*, 26(2):458, 2008.
- [113] L. Jay Guo. Nanoimprint lithography: Methods and material requirements. *Advanced Materials*, 19(4):495–513, 2007.

- [114] Gaute Otnes, Magnus Heurlin, Mariusz Graczyk, Jesper Wallentin, Daniel Jacobsson, Alexander Berg, Ivan Maximov, and Magnus T. Borgström. Strategies to obtain pattern fidelity in nanowire growth from large-area surfaces patterned using nanoimprint lithography. *Nano Research*, 9(10):2852–2861, 2016.
- [115] Harun H. Solak, Christian Dais, and Francis Clube. Displacement Talbot lithography: a new method for high-resolution patterning of large areas. *Optics Express*, 19(11):10686, 2011.
- [116] Víctor J. Gómez, Mariusz Graczyk, Reza Jafari Jam, Sebastian Lehmann, and Ivan Maximov. Wafer-scale nanofabrication of sub-100 nm arrays by deep-UV displacement Talbot lithography. *Nanotechnology*, 31(29):295301, 2020.
- [117] Gerald B. Stringfellow. *Organometallic Vapor-Phase Epitaxy: Theory and Practice*. Academic Press, Cambridge, MA, USA, 1999. ISBN 978-01-267-3842-1.
- [118] Kimberly A. Dick. A review of nanowire growth promoted by alloys and non-alloying elements with emphasis on Au-assisted III–V nanowires. *Progress in Crystal Growth and Characterization of Materials*, 54(3-4):138–173, 2008.
- [119] Yong Kim, Hannah J. Joyce, Qiang Gao, H. Hoe Tan, Chennupati Jagadish, Mohanchand Paladugu, Jin Zou, and Alexandra A. Suvorova. Influence of nanowire density on the shape and optical properties of ternary InGaAs nanowires. *Nano Letters*, 6(4):599–604, 2006.
- [120] Gottfried Zimmermann, Abdallah Ougazzaden, André Gloukhian, Elchuri V. K. Rao, Daniel Delprat, Abderrahim Ramdane, and Andréi Mircea. Selective area MOVPE growth of InP, InGaAs and InGaAsP using TBAs and TBP at different growth conditions. *Journal of Crystal Growth*, 170(1-4):645–649, 1997.
- [121] Magnus T. Borgström, George Immink, Bas Ketelaars, Rienk Algra, and Erik P. A. M. Bakkers. Synergetic nanowire growth. *Nature Nanotechnology*, 2(9):541–544, 2007.
- [122] Kimberly A. Dick, Knut Deppert, Lisa S. Karlsson, L. Reine Wallenberg, Lars Samuelson, and Werner Seifert. A new understanding of Au-assisted growth of III–V semiconductor nanowires. *Advanced Functional Materials*, 15(10):1603–1610, 2005.
- [123] Rajendra P. Gupta, W.S. Khokle, Joachim Wuerfl, and Hans L. Hartnagel. Diffusion of gallium in thin gold films on GaAs. *Thin Solid Films*, 151(3):L121–L125, 1987.
- [124] Magnus Heurlin, Nicklas Anttu, Christian Camus, Lars Samuelson, and Magnus T. Borgström. In situ characterization of nanowire dimensions and growth dynamics by optical reflectance. *Nano Letters*, 15(5):3597–3602, 2015.
- [125] Anwar Ul-Hamid. *A Beginners’ Guide to Scanning Electron Microscopy*. Springer International Publishing, Cham, 2018. ISBN 978-3-319-98481-0.
- [126] C. Blömers, Thomas Grap, Mihail I. Lepsa, Jürgen Moers, Stefan Trelenkamp, Detlev Grützmacher, Hans Lüth, and Thomas Schäpers. Hall effect measurements on InAs nanowires. *Applied Physics Letters*, 101(15):152106, 2012.
- [127] Fredrik Lindelöw, Magnus Heurlin, Gaute Otnes, Vilgailė Dagtė, David Lindgren, Olof Hultin, Kristian Storm, Lars Samuelson, and Magnus T. Borgström. Doping evaluation of InP nanowires for tandem junction solar cells. *Nanotechnology*, 27(6):065706, 2016.

- [128] Xulu Zeng, Renato T. Mourão, Gaute Otnes, Olof Hultin, Vilgailė Dagytė, Magnus Heurlin, and Magnus T. Borgström. Electrical and optical evaluation of n-type doping in  $\text{In}_x\text{Ga}_{1-x}\text{P}$  nanowires. *Nanotechnology*, 29(25):255701, 2018.
- [129] Tuomas Haggren, Gaute Otnes, Renato Mourão, Vilgailė Dagytė, Olof Hultin, Fredrik Lindelöw, Magnus T. Borgström, and Lars Samuelson. InP nanowire p-type doping via Zinc indiffusion. *Journal of Crystal Growth*, 451:18–26, 2016.
- [130] Shermin Arab, Maoqing Yao, Chongwu Zhou, P. Daniel Dapkus, and Stephen B. Cronin. Doping concentration dependence of the photoluminescence spectra of n-type GaAs nanowires. *Applied Physics Letters*, 108(18):182106, 2016.
- [131] Jesper Wallentin. *Doping of Semiconductor Nanowires*. 2013. ISBN 978-91-7473-439-3.
- [132] Enrique Barrigón, Lukas Hrachowina, and Magnus T. Borgström. Light current-voltage measurements of single, as-grown, nanowire solar cells standing vertically on a substrate. *Nano Energy*, 78:105191, 2020.
- [133] Igor Vurgaftman, J. R. Meyer, and L. Ramdas Ram-Mohan. Band parameters for III–V compound semiconductors and their alloys. *Journal of Applied Physics*, 89(11):5815–5875, 2001.
- [134] Timothy H. Gfroerer. Photoluminescence in analysis of surfaces and interfaces. In *Encyclopedia of Analytical Chemistry*, pages 9209–9231. John Wiley & Sons, Ltd, 2006. ISBN 978-0-471-97670-7.
- [135] Asmita Jash, Aymen Yangui, Sebastian Lehmann, Ivan G. Scheblykin, Kimberly A. Dick, Anders Gustafsson, and Mats-Erik Pistol. Time-resolved photoluminescence studies of single interface wurtzite/zincblende heterostructured InP nanowires. *Applied Physics Letters*, 120(11):113102, 2022.
- [136] Lyubov V. Titova, Thang B. Hoang, Jan M. Yarrison-Rice, Howard E. Jackson, Yong Kim, Hannah J. Joyce, Qiang Gao, H. Hoe Tan, Chennupati Jagadish, Xin Zhang, Jin Zou, and Leigh M. Smith. Dynamics of strongly degenerate electron–hole plasmas and excitons in single InP nanowires. *Nano Letters*, 7(11):3383–3387, 2007.
- [137] Hannah J. Joyce, Qiang Gao, H. Hoe Tan, Chennupati Jagadish, Yong Kim, Melodie A. Fickenscher, Saranga Perera, Thang Ba Hoang, Leigh M. Smith, Howard E. Jackson, Jan M. Yarrison-Rice, Xin Zhang, and Jin Zou. Unexpected benefits of rapid growth rate for III–V nanowires. *Nano Letters*, 9(2):695–701, 2009.
- [138] Vilgailė Dagytė, Enrique Barrigón, Wei Zhang, Xulu Zeng, Magnus Heurlin, Gaute Otnes, Nicklas Anttu, and Magnus T. Borgström. Time-resolved photoluminescence characterization of GaAs nanowire arrays on native substrate. *Nanotechnology*, 28(50):505706, 2017.
- [139] Lachlan E. Black, Alessandro Cavalli, Marcel A. Verheijen, Jos E. M. Haverkort, Erik P. A. M. Bakkers, and Wilhelmus M. M. Kessels. Effective surface passivation of InP nanowires by atomic-layer-deposited  $\text{Al}_2\text{O}_3$  with  $\text{PO}_x$  interlayer. *Nano Letters*, 17(10):6287–6294, 2017.

- [140] Zhiqin Zhong, Ziyuan Li, Qian Gao, Zhe Li, Kun Peng, Li Li, Sudha Mokkaapati, Kaushal Vora, Jiang Wu, Guojun Zhang, Zhiming Wang, Lan Fu, Hark Hoe Tan, and Chennupati Jagadish. Efficiency enhancement of axial junction InP single nanowire solar cells by dielectric coating. *Nano Energy*, 28:106–114, 2016.
- [141] Lukas Hrachowina, Xianshao Zou, Yang Chen, Yuwei Zhang, Enrique Barrigón, Arkady Yartsev, and Magnus T. Borgström. Imaging the influence of oxides on the electrostatic potential of photovoltaic InP nanowires. *Nano Res.*, 14:4087–4092, 2021.
- [142] Simonpietro Agnello. *Spectroscopy for Materials Characterization*. Wiley, 2021. ISBN 978-1-119-69732-9.
- [143] Gaute Otnes, Enrique Barrigón, Christian Sundvall, K. Erik Svensson, Magnus Heurlin, Gerald Siefer, Lars Samuelson, Ingvar Åberg, and Magnus T. Borgström. Understanding InP nanowire array solar cell performance by nanoprobe-enabled single nanowire measurements. *Nano Letters*, 18(5):3038–3046, 2018.
- [144] Yang Chen, Pyry Kivisaari, Mats-Erik Pistol, and Nicklas Anttu. Optimized efficiency in InP nanowire solar cells with accurate 1D analysis. *Nanotechnology*, 29(4):045401, 2018.
- [145] Dennis Hausmann, Jill Becker, Shenglong Wang, and Roy G. Gordon. Rapid vapor deposition of highly conformal silica nanolaminates. *Science*, 298:402–406, 2002.
- [146] Jenny A. Nelson. *The Physics of Solar Cells*. World Scientific Publishing Company, 2003. ISBN 1-84816-823-3.
- [147] Clemens Vierheilig, Ulrich T. Schwarz, Nikolaus Gmeinwieser, Ansgar Laubsch, and Berthold Hahn. Bias dependent spatially resolved photoluminescence spectroscopy and photocurrent measurements of InGaN/GaN LED structures. *physica status solidi c*, 6 (S2):S755 – S758, 2009.
- [148] Zhihua Xu, Taryn De Rosia, and Kevin Weeks. Photoluminescence–voltage (PL–V) hysteresis of perovskite solar cells. *The Journal of Physical Chemistry C*, 121(44):24389–24396, 2017.
- [149] Cesare Donolato. Theory of beam induced current characterization of grain boundaries in polycrystalline solar cells. *Journal of Applied Physics*, 54(3):1314–1322, 1983.
- [150] Jürgen Carstensen, George Popkirov, Jacqueline Bahr, and Helmut Föll. CELLO: an advanced LBIC measurement technique for solar cell local characterization. *Solar Energy Materials and Solar Cells*, 76(4):599–611, 2003.
- [151] Amanda Kaminski, Otwin Breitenstein, J. P. Boyeaux, Pati Rakotoniaina, and A. Laugier. Light beam induced current and infrared thermography studies of multicrystalline silicon solar cells. *Journal of Physics: Condensed Matter*, 16:S9–S18, 2004.
- [152] Uwe Rau. Reciprocity relation between photovoltaic quantum efficiency and electroluminescent emission of solar cells. *Physical Review B*, 76(8):085303, 2007.
- [153] Thomas Kirchartz, Anke Helbig, Wilfried Reetz, Michael Reuter, Jürgen H. Werner, and Uwe Rau. Reciprocity between electroluminescence and quantum efficiency used for the characterization of silicon solar cells. *Progress in Photovoltaics: Research and Applications*, 17(6):394–402, 2009.

- [154] David Hinken, Klaus Ramspeck, Karsten Bothe, Bernhard Fischer, and Rolf Brendel. Series resistance imaging of solar cells by voltage dependent electroluminescence. *Applied Physics Letters*, 91(18):182104, 2007.
- [155] Jonas Haunschild, Markus Glatthaar, Martin Kasemann, Stefan Rein, and Eicke R. Weber. Fast series resistance imaging for silicon solar cells using electroluminescence. *physica status solidi (RRL) – Rapid Research Letters*, 3(7-8):227–229, 2009.
- [156] Otwin Breitenstein, Archita Khanna, Yael Augarten, Jan Bauer, Jan-Martin Wagner, and Kornelius Iwig. Quantitative evaluation of electroluminescence images of solar cells. *physica status solidi (RRL) – Rapid Research Letters*, 4(1-2):7–9, 2010.
- [157] Lukas Hrachowina, Nicklas Anttu, and Magnus T. Borgström. Wafer-scale synthesis and optical characterization of InP nanowire arrays for solar cells. *Nano Letters*, 21(17):7347–7353, 2021.
- [158] Jiuru Sun and Jacek J. Jasieniak. Semi-transparent solar cells. *Journal of Physics D: Applied Physics*, 50(9):093001, 2017.
- [159] T. Miyazaki, A. Akisawa, and T. Kashiwagi. Energy savings of office buildings by the use of semi-transparent solar cells for windows. *Renewable Energy*, 30(3):281–304, 2005.
- [160] Yepin Zhao, Yuan Zhu, Hao-Wen Cheng, Ran Zheng, Dong Meng, and Yang Yang. A review on semitransparent solar cells for agricultural application. *Materials Today Energy*, 22:100852, 2021.
- [161] Jae Choul Yu, Bin Li, Christopher J. Dunn, Junlin Yan, Benjamin T. Diroll, Anthony S. R. Chesman, and Jacek J. Jasieniak. High-performance and stable semi-transparent perovskite solar cells through composition engineering. *Advanced Science*, 9(22):2201487, 2022.
- [162] Yang Chen, Mats-Erik Pistol, and Nicklas Anttu. Design for strong absorption in a nanowire array tandem solar cell. *Scientific Reports*, 6(1), 2016.
- [163] Ian M. Peters, Carlos D. Rodríguez Gallegos, Larry Lüer, Jens A. Hauch, and Christoph J. Brabec. Practical limits of multijunction solar cells. *Progress in Photovoltaics: Research and Applications*, 31(10):1006–1015, 2023.
- [164] Manuel Schnabel, Michael Rienacker, Emily L. Warren, John F. Geisz, Robby Peibst, Paul Stradins, and Adele C. Tamboli. Equivalent performance in three-terminal and four-terminal tandem solar cells. *IEEE Journal of Photovoltaics*, 8(6):1584–1589, 2018.
- [165] Simon P. Philipps, Frank Dimroth, and Andreas W. Bett. High-efficiency III–V multijunction solar cells. In *McEvoy’s Handbook of Photovoltaics*, pages 439–472. Elsevier, 2018. ISBN 978-0-12-809921-6.
- [166] Vilgailė Dagytė, Magnus Heurlin, Xulu Zeng, and Magnus T. Borgström. Growth kinetics of  $\text{Ga}_x\text{In}_{1-x}\text{P}$  nanowires using triethylgallium as Ga precursor. *Nanotechnology*, 29(39):394001, 2018.
- [167] Gaute Otnes, Magnus Heurlin, Xulu Zeng, and Magnus T. Borgström.  $\text{In}_x\text{Ga}_{1-x}\text{P}$  nanowire growth dynamics strongly affected by doping using diethylzinc. *Nano Letters*, 17(2):702–707, 2017.

- [168] Alexander Berg, Filip Lenrick, Neimantas Vainorius, Jason P. Beech, L. Reine Wallenberg, and Magnus T. Borgström. Growth parameter design for homogeneous material composition in ternary  $\text{Ga}_x\text{In}_{1-x}\text{P}$  nanowires. *Nanotechnology*, 26(43):435601, 2015.
- [169] Daniel Jacobsson, Johan M. Persson, Dominik Kriegner, Tanja Etzelstorfer, Jesper Wallentin, Jakob B. Wagner, Julian Stangl, Lars Samuelson, Knut Deppert, and Magnus T. Borgström. Particle-assisted  $\text{Ga}_x\text{In}_{1-x}\text{P}$  nanowire growth for designed bandgap structures. *Nanotechnology*, 23(24):245601, 2012.
- [170] Jesper Wallentin, Laura Barrutia Poncela, Anna M. Jansson, Kilian Mergenthaler, Martin Ek, Daniel Jacobsson, L. Reine Wallenberg, Knut Deppert, Lars Samuelson, Dan Hessman, and Magnus T. Borgström. Single GaInP nanowire p-i-n junctions near the direct to indirect bandgap crossover point. *Applied Physics Letters*, 100(25):251103, 2012.
- [171] Wei Zhang, Xulu Zeng, Xiaojun Su, Xianshao Zou, Pierre-Adrien Mante, Magnus T. Borgström, and Arkady Yartsev. Carrier recombination processes in gallium indium phosphide nanowires. *Nano Letters*, 17(7):4248–4254, 2017.

# Scientific publications



# Paper I

**D. Alcer**, L. Hrachowina, D. Hessman, and M. T. Borgström

Processing and characterization of large area InP nanowire photovoltaic devices  
*Nanotechnology* 34, 295402 (2023)

Reproduced with permission from *IOP Publishing*

© 2023 The authors. Published by IOP Publishing. Licensed under CC-BY 4.0.

The paper can be accessed at:

<https://doi.org/10.1088/1361-6528/accc37>



A link to the supplementary information is available under the name “Supplementary data” on the same webpage.



## Paper II

Y. Chen, L. Hrachowina, E. Barrigon, J. P. Beech, **D. Alcer**, R. Lyttleton,  
R. Jafari Jam, L. Samuelson, H. Linke, and M. T. Borgström  
Semiconductor nanowire array for transparent photovoltaic applications  
Applied Physics Letters 118, 191107 (2021)  
Reproduced with permission from *AIP Publishing*  
© 2021 AIP Publishing

The paper can be accessed at:

<https://doi.org/10.1063/5.0046909>



The supplementary information is available under this link:

[https://pubs.aip.org/apl/article-supplement/1062613/zip/191107\\_1\\_supplements/](https://pubs.aip.org/apl/article-supplement/1062613/zip/191107_1_supplements/)





# Paper III

**D. Alcer**, A. P. Saxena, L. Hrachowina, X. Zou, A. Yartsev, and M. T. Borgström  
Comparison of triethylgallium and trimethylgallium precursors for GaInP nano-  
wire growth  
*Physica Status Solidi B*, 2000400 (2020)  
Reproduced with permission from *Wiley-VCH*  
© 2023 The authors. Published by Wiley-VCH. Licensed under CC-BY 4.0.

The paper can be accessed at:

<https://doi.org/10.1002/pssb.202000400>



The supplementary information is available under this link:

<https://onlinelibrary.wiley.com/action/downloadSupplement?doi=10.1002%2Fpssb.202000400&file=pssb202000400-sup-0001-SuppData-S1.docx>





# Paper IV

**D. Alcer**, M. Tirrito, L. Hrachowina, and M. T. Borgström

Vertically processed GaInP/InP tandem-junction nanowire solar cells

ACS Applied Nano Materials 7, 2352–2358 (2024)

Reproduced with permission from *American Chemical Society*

© 2024 The authors. Published by American Chemical Society. Licensed under CC-BY 4.0.

The paper can be accessed at:

<https://doi.org/10.1021/acsanm.3c05909>



The supplementary information is available under this link:

[https://pubs.acs.org/doi/suppl/10.1021/acsanm.3c05909/suppl\\_file/an3c05909\\_si\\_001.pdf](https://pubs.acs.org/doi/suppl/10.1021/acsanm.3c05909/suppl_file/an3c05909_si_001.pdf)





**LUND**  
UNIVERSITY

Faculty of Engineering, LTH  
Department of Physics  
Division of Solid State Physics

ISBN 978-91-8039-960-9

